J|A|C|S ARTICLES

Published on Web 10/14/2009

Molecular Alloys, Linking Organometallics with Intermetallic Hume−Rothery Phases: The Highly Coordinated Transition Metal Compounds $[M(ZnR)_n]$ ($n \geq 8$) Containing Organo−Zinc Ligands

Thomas Cadenbach,[†] Timo Bollermann,[†] Christian Gemel,[†] Mustafa Tombul,[†] Israel Fernandez,[‡] Moritz von Hopffgarten,[§] Gernot Frenking,*[,§] and Roland A. Fischer*[,†]

Inorganic Chemistry II - Organometallics & Materials, Faculty of Chemistry and Biochemistry, Ruhr University Bochum, D-44870 Bochum, Germany, Departamiento Química Orgánica, Facultad de Química, Universidad Complutense de Madrid, 28040 Madrid, Spain, and Department of Chemistry, Philipps-University Marburg, D-35032 Marburg, Germany

Received May 19, 2009; E-mail: roland.fischer@rub.de; frenking@chemie.uni-marburg.de

Abstract: This paper presents the preparation, characterization and bonding analyses of the closed shell 18 electron compounds $[M(ZnR)_n]$ (M = Mo, Ru, Rh, Ni, Pd, Pt, $n = 8-12$), which feature covalent bonds between n one-electron organo-zinc ligands ZnR (R = Me, Et, η^5-$C_5(CH_3)_5$ = Cp*) and the central metal M. The compounds were obtained in high isolated yields (>80%) by treatment of appropriate GaCp* containing transition metal precursors **13-18**, namely $[Mo(GaCp^*)_6]$, $[Ru_2(Ga)(GaCp^*)_7(H)_3]$ or $[Ru(GaCp^*)_6(Cl)_2]$, $[(Cp^*Ga)_4RhGa(\eta^1\text{-}Cp^*)Me]$ and $[M(GaCp^*)_4]$ (M = Ni, Pd, Pt) with $ZnMe_2$ or $ZnEt_2$ in toluene solution at elevated temperatures of 80−110 °C within a few hours of reaction time. Analytical characterization was done by elemental analyses (C, H, Zn, Ga), ^{1}H and ^{13}C NMR spectroscopy. The molecular structures were determined by single crystal X-ray diffraction. The coordination environment of the central metal M and the M−Zn and Zn−Zn distances mimic the situation in known solid state M/Zn Hume−Rothery phases. DFT calculations at the RI-BP86/def2-TZVPP and BP86/TZ2P+ levels of theory, AIM and EDA analyses were done with $[M(ZnH)_n]$ (M = Mo, Ru, Rh, Pd; $n = 12, 10, 9, 8$) as models of the homologous series. The results reveal that the molecules can be compared to 18 electron gold clusters of the type $M@Au_n$, that is, $W@Au_{12}$, but are neither genuine coordination compounds nor interstitial cage clusters. The molecules are held together by strong radial M−Zn bonds. The tangential Zn−Zn interactions are generally very weak and the $(ZnH)_n$ cages are not stable without the central metal M.

Introduction

Probing and pushing the limits of metal-to-metal bonding has continuously been a strong motivation for the explorative synthetic chemist since the pioneering work of the sixties on metal clusters and metal multiple bonding.[1] Quite recent and spectacular reports such as the chromium−chromium quintuple bond[2] and the zinc−zinc single bond[3] in organometallic molecules show that there is still plenty of room for new discoveries. A key to success over the last three decades has been the development of tailored steric shielding together with fine-tuning the electronic properties of the ancillary organic substituents at low coordinated metal centers across the periodic table. This concept has been particularly fruitful for Lewis basic carbenoid group-13 and group-14 compounds. Their accessibility on a preparative scale[4,5] stimulated a renaissance of the corresponding coordination chemistry of main group and transition metals by the mid 1990s.[6,7] Parallel to this, certain compounds featuring transition metal to group-13 metal bonds were studied as precursors for the soft chemical synthesis of

* To whom correspondence should be addressed. Email: and
† Ruhr University Bochum.
‡ Universidad Complutense de Madrid.
§ Philipps-University Marburg.

(1) (a) Cotton, F. A.; Curtis, N. F.; Harris, C. B.; Johnson, B. F. G.; Lippard, S. J.; Mague, J. T.; Robinson, W. R.; Wood, J. S. *Science* **1964**, *145*, 1305–1307. (b) Cotton, F. A.; MurilloL. A.; Walton, R. A. *Multiple Bonds Between Metal Atoms*, 3rd ed.; Springer: Berlin, 2005.
(2) Nguyen, T.; Sutton, A. D.; Brynda, M.; Fettinger, J. C.; Long, G. L.; Power, P. P. *Science* **2005**, *310*, 844–847.
(3) (a) Resa, I.; Carmona, E.; Gutierrez-Puebla, E.; Monge, A. *Science* **2004**, *305*, 1136–1138. (b) Kays, D. L.; Aldridge, S. *Angew. Chem., Int. Ed.* **2009**, *48*, 4109–4111.
(4) Baker, R. J.; Jones, C. *Coord. Chem. Rev.* **2005**, *249*, 1857–1869.
(5) Nagendran, S.; Roesky, H. W. *Organometallics* **2008**, *27*, 457–492.
(6) (a) Fischer, R. A.; Weiss, J. *Angew. Chem., Int. Ed* **1999**, *38*, 2830–2850. (b) Linti, G.; Schnöckel, G.; H. *Coord. Chem. Rev.* **2000**, *206−207*, 285–319. (c) Gemel, C.; Steinke, T.; Cokoja, M.; Kempter, A.; Fischer, R. A. *Eur. J. Inorg. Chem.* **2004**, 4161–4176. (d) Himmel, H.-J.; Linti, H.-J. G. *Angew. Chem., Int. Ed.* **2008**, *47*, 6326–6328. (e) Kays, D. L; Aldridge, S. *Struct. Bonding* **2008**, *130*, 29–122. (f) Roesky, P. W. *Dalton Trans.* **2009**, 1887–1893.
(7) (a) Okazaki, M.; Tobita, H.; Ogino, H. *Dalton Trans.* **2003**, 493–506. (b) Kira, M. *Organomet. News* **2007**, 76–81.
(8) (a) Hume-Rothery, W. *J. Inst. Met.* **1926**, *35*, 295–361. (b) Jones, H. *Proc. Phys. Soc.* **1937**, *49*, 250–257. (c) Paxton, A.; Methfessel, M.; Pettifor, D. *Proc. R. Soc. London, Ser. A* **1997**, *453*, 1493–1514. (d) Ferro, R. A.; Saccone, A. in *Materials Science and Technology Vol. 1, The Structure of Solids*; Cahn, R. W., Haasen, P., Kramer, E. J., Eds.; VCH, Weinheim, 1993, pp. 123−215.

the respective Hume−Rothery phases[8] deposited as thin films on substrates (e.g., CoGa, NiIn)[9] or dispersed as nanoparticles in non aqueous colloidal solution (e.g., "nano-brass" CuZn; "nano-bronze" CuAl; NiAl).[10] Homoleptic mixed-metal cluster-type compounds of the general formula $[M_a(ER)_b]$ (E = Al, Ga, In; R = η^5-C_5Me_5 = Cp*)[6c] became available during the past few years and are particularly interesting within the scope of precursor chemistry. In this context, the Cp* group is preferred to other possible substituents R because of its medium-scale steric bulk and soft binding properties which allows higher coordination numbers (e.g., $b \gg a$) together with the possibility to cleave Cp* from the group-13 metal in a smooth and controlled way.[11] Zinc, similar to aluminum and gallium, is an important metallurgical element and a component of classical alloy materials such as common brass. With transition metals it forms a rich variety of binary and ternary intermetallic solid state compounds of complex compositions and structures. For example, the metal atoms of the zinc rich Hume−Rothery γ-phase, Cu_5Zn_8, are distributed over four distinct crystallographic sites, two exhibit an icosahedral local environment while the other two sites are surrounded by eleven and thirteen vertex polyhedra of lower symmetry.[12] This situation however, has no parallel in the molecular chemistry of zinc. A moderate number of transition metal zinc complexes featuring covalent

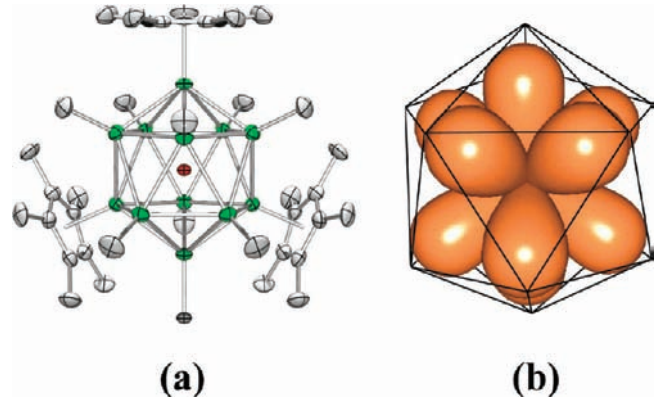

Figure 1. $[Mo(ZnCp^*)_3(ZnMe)_9]$ and the sd^5 hybridized Mo center.

M−Zn bonds are known,[13] but zinc rich cluster-like molecular compounds do not exist.[14] Zinc and Gallium are neighbors in the periodic table and have comparable atomic volumes and electronegativities (1.7 and 1.8 for Zn and Ga respectively on the Allred-Rochow scale). From the viewpoint of simple electron counting rules in coordination chemistry, one GaCp* acting as a 2 electron donor ligand may be regarded as equivalent to two ZnCp* serving as 1 electron donor ligands for binding to a transition metal center. By looking at the synthesis of [Cp*Zn−ZnCp*] from $ZnCp^*_2$ and $ZnEt_2$,[3] taking into account the reducing power of GaCp* and recognizing the fact, that zinc can substitute gallium in intermetallic compounds to some extent,[15] we were lead to investigate the reaction of $[L_mM(GaCp^*)_n]$ (L = CO and/or all-hydrocarbon π-ligands) compounds with ZnR_2 (R = Me, Et). In the course of these studies we discovered two unusual very zinc-rich molybdenum complexes, that is, $[Mo(ZnCp^*)_3(ZnMe)_9]$ and $[\{Mo(CO)_4\}_4(Zn)_6(\mu-ZnCp^*)_4]$. Their molecular structures indeed represent cut-outs of the known solid state phase $MoZn_{22.4}$, which in fact supports the idea of deriving novel molecular models for alloy (nano) materials from this chemistry, as is suggested by the title.[16,17]

The crystal structure of $[Mo(ZnCp^*)_3(ZnMe)_9]$ exhibits an icosahedral closed packed $MoZn_{12}$ core with a central Mo atom and a C_3 symmetric arrangement of the hydrocarbon substituents (Me, Cp*) at the periphery (Figure 1).[16] The isolobal relationship H/ZnR and the corresponding chemical analogy H/Au[18] allows the comparison between the new $MoZn_{12}$ system with homo-

(9) (a) Fischer, R. A.; Kaesz, H. D.; Khan, S. I.; Muller, H. J. *Inorg. Chem.* **1990**, *29*, 1601–1602. (b) Fischer, R.; Scherer, W.; Kleine, M. *Angew. Chem., Int. Ed.* **1993**, *32*, 748–750. (c) Fischer, R. A.; Priermeier, T. *Organometallics* **1994**, *13*, 4306–4314. (d) Fischer, R. A.; Miehr, A.; Schulte, M. M. *Adv. Mater.* **1995**, *7*, 58–61. Fischer, R. A.; Miehr, A. *Chem. Mater.* **1996**, *8*, 497–508. (e) Fischer, R. A.; Miehr, A.; Metzger, T. *Thin Solid Films* **1996**, *289*, 147–152. (f) Miehr, A.; Fischer, R. A.; Lehmann, O.; Stuke, M. *Adv. Mat. Optics Electr.* **1996**, *6*, 27–32. (g) Fischer, R. A.; Weiss, J.; Rogge, W. *Polyhedron* **1998**, *17*, 1203–1210. (h) Fischer, R. A.; Weiss, D.; Winter, M.; Muller, I.; Kaesz, H. D.; Fröhlich, N.; Frenking, G. *J. Organomet. Chem.* **2004**, *689*, 4611–4623.

(10) (a) Cokoja, M.; Jagirdar, B. R.; Parala, H.; Birkner, A.; Fischer, R. A. *Eur. J. Inorg. Chem.* **2008**, *333*, 0–3339. (b) Cokoja, M.; Parala, H.; Birkner, A.; Shekhah, O.; van den Berg, M. W. E.; Fischer, R. A. *Chem. Mater.* **2007**, *19*, 5721–5733.

(11) Buchin, B.; Gemel, C.; Cadenbach, T.; Fernandez, I.; Frenking, G.; Fischer, R. A. *Angew. Chem., Int. Ed.* **2006**, *45*, 5207–5210.

(12) Brandon, J. K.; Brizard, R. Y.; Chieh, P. C.; McMillan, R.; KPearson, W. B. *Acta Crystallogr., Sect. B: Struct. Crystallogr. Crystal Chem.* **1974**, *30*, 1412.

(13) (a) Budzelaar, P. H. M.; Boersma, J. ; Van der Kerk, G. J. M. *J. Organomet. Chem.* **1980**, *202*, C71–C72. (b) Budzelaar, P. H. M.; Boersma, J.; Van der Kerk, G. J. M.; Spek, A. L.; Duisenberg, A. J. M. *Inorg. Chem.* **1982**, *21*, 3777–3780. (c) Budzelaar, P. H. M.; Boersma, J.; Van der Kerk, G. J. M. *Angew. Chem.* **1983**, *95*, 335–336. (d) Budzelaar, P. H. M.; Den Haan, K. H.; Boersma, J.; Van der Kerk, G. J. M.; Spek, A. L. *Organometallics* **1984**, *3*, 156–159. (e) Budzelaar, P. H. M.; Van der Zeijden, A. A. H.; Boersma, J.; Van der Kerk, G. J. M.; Spek, A. L.; Duisenberg, A. J. M. *Organometallics* **1984**, *3*, 159–163. (f) Budzelaar, P. H. M.; Boersma, J.; Van der Kerk, G. J. M.; Spek, A. L.; Duisenberg, A. J. M. *J. Organomet. Chem.* **1985**, *287*, C13–C17. (g) Budzelaar, P. H. M.; Boersma, J.; Van der Kerk, G. J. M.; Spek, A. L.; Duisenberg, A. J. M. *Organometallics* **1985**, *4*, 680–683. (h) Fischer, B.; Boersma, J.; Van Koten, G.; Spek, A. L. *N. J. Chem.* **1988**, *12*, 613–620. (i) Fischer, B.; Kleijn, H.; Boersma, J.; Van Koten, G.; Spek, A. L. *Organometallics* **1989**, *8*, 920–925. (j) Fryzuk, M. D.; McConville, D. H.; Rettig, S. J. *Organometallics* **1990**, *9*, 1359–1360. (k) Fryzuk, M. D.; McConville, D. H.; Rettig, S. J. *Organometallics* **1993**, *12*, 2152–2161. (l) Ohashi, M.; Matsubara, K.; Iizuka, T.; Suzuki, H. *Angew. Chem., Int. Ed.* **2003**, *42*, 937–940. (m) Ohashi, M.; Matsubara, K.; Suzuki, H. *Organometallics* **2007**, *26*, 2330–2339, and references therein. (n) Wang, Y.; Quillian, B.; Wannere, C. S.; Wei, P.; Schleyer, P. v. R.; Robinson, G. H. *Organometallics* **2007**, *26*, 3054–3056. (o) Fafard, C. M.; Chen, C.-H.; Foxman, B. M.; Ozerov, O. V. *Chem. Comm.* **2007**, 4465. (p) Crotty, D. E.; Corey, E. R.; Anderson, T. J.; Glick, M. D.; Oliver, J. R. *Inorg. Chem.* **1977**, *16*, 920–924. (q) Crotty, D. E.; Anderson, T. J.; Glick, M. D.; Oliver, J. R. *Inorg. Chem.* **1977**, *16*, 2346–2350.

(14) Zhen, S.; Seff, K. *J. Phys. Chem. B.* **1999**, *103*, 6493.

(15) (a) Viklund, P.; Svensson, C.; Hull, S.; Simak, S. I.; Berastegui, P.; Haussermann, U. *Chem.−Eur. J.* **2001**, *7*, 5143. (b) Häussermann, U.; Viklund, P.; Svensson, C.; Eriksson, S.; Berastegui, P.; Lidin, S. *Angew. Chem., Int. Ed.* **1999**, *38*, 488–492.

(16) Cadenbach, T.; Bollermann, T.; Gemel, C.; Fernandez, I.; von Hopffgarten, M.; Frenking, G.; Fischer, R. A. *Angew. Chem., Int. Ed.* **2008**, *47*, 9150–9154.

(17) Cadenbach, T; Gemel, C.; Fischer, R. A. *Angew. Chem., Int. Ed.* **2008**, *47*, 9146–9149.

(18) (a) Kiran, B.; Li, X.; Zhai, H.-J.; Cui, L.-F.; Wang, L.-S. *Angew. Chem., Int. Ed.* **2004**, *43*, 2125–2129. (b) Gagliardi, L.; Pyykkö, P. *Phys. Chem. Chem. Phys.* **2004**, *6*, 2904–2906.

(19) (a) Gagliardi, L.; Pyykkö, P. *J. Am. Chem. Soc.* **2004**, *126*, 15014–15015. (b) Wang, X.; Andrews, L.; Infante, I.; Gagliardi, L. *J. Am. Chem. Soc.* **2008**, *130*, 1972–1978. (c) Infante, I.; Gagliardi, L.; Wang, X.; Andrews, L. *J. Phys. Chem. A* **2009**, *113*, 2446–2455.

(20) (a) Li, X.; Kiran, B.; Li, J.; Zhai, H.-J.; Wang, L.-S. *Angew. Chem., Int. Ed.* **2002**, *41*, 4786; *Angew Chem.* **2002**, *114*, 4980−4983. (b) Pyykko, P.; Runeberg, N. *Angew. Chem., Int. Ed.* **2002**, *41*, 2174–2176. (c) Autschbach, J.; Hess, B. A.; Johansson, M. P.; Neugebauer, J.; Patzschke, M.; Pyykkö, P.; Reiher, M.; Sundholm, D. *Phys. Chem. Chem. Phys.* **2004**, *6*, 11–22.

Table 1. Composition and Numbering Scheme of the Compounds **1**−**12**

number[a]	composition[b]	core	c.n.	symmetry[c]
1 (**1H**)	[Mo(ZnCp*)$_3$(ZnMe)$_9$]	[MoZn$_{12}$	12	[C_3(I_h)
2	[Mo(ZnCp*)$_2$(ZnEt)$_{10}$]	MoZn$_{12}$	12	C_s
3	[Mo(GaMe)$_4$(ZnCp*)$_4$]	MoGa$_4$Zn$_4$	8	T_d
4	[Mo(GaMe)$_2$(ZnCp*)$_4$(ZnMe)$_4$]	MoGa$_2$Zn$_8$	10	C_s
5 (**5H**)	[Ru(ZnCp*)$_4$(ZnMe)$_6$]	RuZn$_{10}$	10	C_3(D_{4d})
6	[Ru(ZnCp*)$_4$(ZnMe)$_4$(H)$_2$]	RuZn$_8$H$_2$	10	T_d
7 (**7H**)	[Rh(ZnCp*)$_3$(ZnMe)$_6$]	RhZn$_9$	9	C_3(D_{3h})
8	[Rh(GaMe)(ZnCp*)$_4$(ZnMe)$_3$]	RhGaZn$_7$	8	C_3
9 (**9H**)	[Ni(ZnCp*)$_4$(ZnMe)$_4$]	NiZn$_8$	8	(D_{4d})
10 (**10H**)	[Pd(ZnCp*)$_4$(ZnMe)$_4$]	PdZn$_8$	8	T_d(D_{4d})
11 (**11H**)	[Pt(ZnCp*)$_4$(ZnMe)$_4$]	PtZn$_8$	8	T_d(D_{4d})
12	[Pt(ZnCp*)$_4$(ZnEt)$_4$]	PtZn$_8$	8	T_d(D_{4d})

[a] Numbers in parentheses, **1H** etc., refer to the model systems of the general formula [M(ZnH)$_n$] where Cp* and Me, Et groups were replaced by H. These simplified structures were used for the quantum chemical calculations. [b] All compounds −**12** fulfill the 18 electron rule by counting the ZnR as one electron and GaR as two electron ligands at the metal center M. [c] Symbols refer to the idealized (local) point group symmetry of the compounds.

leptic highly coordinated d/f-metal hydride species such as WH$_{12}$,[19] and the 18 electron cluster WAu$_{12}$.[20] These latter species have been observed in matrix studies or in the gas phase (but are not accessible in preparative quantities in ambient conditions). The quantum chemical analysis of the electronic structure of [Mo(ZnCp*)$_3$(ZnMe)$_9$], however, revealed an unprecedented situation. It can be described as a perfectly sd^5 hybridized central Mo atom where all 12 lobes of the hybrid orbitals are used for chemical bonding (Figure 1). From this point of view, the molecule is held together by six three-center two-electron Zn−Mo−Zn electron-sharing bonds across the diagonals of the MoZn$_{12}$ core. Thus, the compound turned out to be neither a genuine complex which is defined by donor−acceptor bonds between closed-shell species nor a born-out interstitial cluster where bonding interaction is mainly between the cage atoms. Rather, the bonding situation is characterized by weak tangential Zn−Zn bonding which only supports a hitherto unknown MoZn$_{12}$ core with strong radial Mo−Zn interactions. This is different from the MH$_{12}$ and MAu$_{12}$ cases mentioned above.[19,20] Expansion of the principle to transition metal centers other than molybdenum obviously seems feasible, because (homoleptic) complexes such as [M(GaCp*)$_n$] are available for many transition metals M. In this paper we now wish to report on the synthesis, structural characterization and elucidation of the bonding situation by means of DFT calculation of a series of homoleptic, 18 electron compounds of the general formula [M(ZnR)$_n$] ($n \geq 8$; R = Me, Et, Cp*) for a selection of transition metals M = Mo, Ru, Rh, Ni, Pd and Pt (Table 1).

Results

1. Synthesis and Structural Characterization of the New Compounds. The title compounds **1**−**12** of the general formula [M(ZnR)$_n$(GaMe)$_m$] ($n + m = 8-12$; M = Mo, Ru, Rh, Ni, Pd, Pt; R = CH$_3$, Cp*; for the numbering scheme, see Table 1) are formed by the treatment of the all-gallium coordinated transition metal precursors [Mo(GaCp*)$_6$] (**13**),[21] [Ru$_2$(Ga)(GaCp*)$_7$(H)$_3$] (**14**)[22] or [Ru(GaCp*)$_6$(Cl)$_2$] (**15**),[23]

Scheme 1. Synthesis of the Compounds **1**−**12**

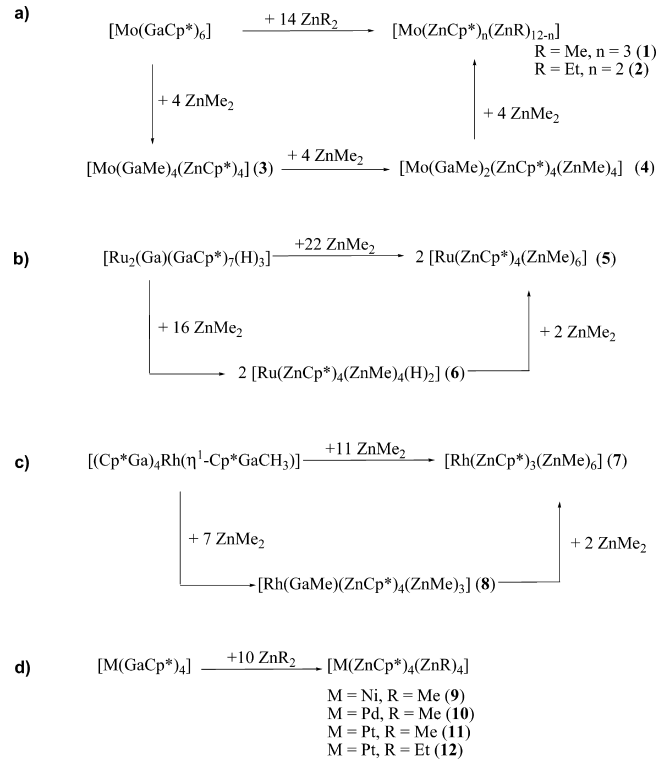

[(Cp*Ga)$_4$RhGa(η^1-Cp*)Me] (**16**)[24] and [M(GaCp*)$_4$] (**17**−**18**; M = Ni, Pd, Pt)[25] with a suitably chosen excess of ZnMe$_2$ or ZnEt$_2$ in toluene solution at elevated temperatures of 80−110 °C within a few hours of reaction time (Scheme 1). The isolated yields were usually quite good, and the selectivities of the reactions were very high (NMR of the reaction solutions). All new compounds were fully characterized by ^{1}H and ^{13}C NMR spectroscopy, elemental micro analysis (C, H, Ga and Zn) and single-crystal X-ray crystallography. The molecular structures (Figure 2) of all new compounds **1**−**12** correspond to typical deltahedral coordination polyhedra, namely icosahedron, bi-capped square antiprism, capped square antiprism and dodecahedron, in accordance with a straightforward deduction from the VSEPR concept. However, the distinction of Zn vs Ga in the coordination sphere around the central metal M of **3**, **4** and **8** cannot be done by X-ray single crystal structure analysis without ambiguity because Zn and Ga are neighbors in the periodic table and have very similar electron densities and X-ray scattering properties. Certainly, a distinction between Zn and Ga can be made by single-crystal neutron diffraction studies. However, this technique is particularly difficult to apply in our case. The presence of Ga was ruled out by analysis of the metal content using atomic absorption spectroscopy for the all-zinc coordinated compounds **1**−**2**, **5**−**7**, and **10**−**12**. The compositions of the Zn/Ga mixed compounds **3**−**4** and **8** have been determined by total elemental analysis. The sensitivity of the new compounds to air and traces of water ruled out the unambiguous confirmation of the composition by high resolution mass spectroscopy techniques (e.g., using electron spray ionization, ESI), at least in our hands so far.

(21) Cadenbach, T. Ph.D. thesis, Ruhr-University, Bochum, 2009.
(22) Cadenbach, T.; Gemel, C.; Schmid, R.; Halbherr, M.; Yusenko, K.; Cokoja, M.; Fischer, R. A. *Angew. Chem., Int. Ed.* **2009**, *48*, 3872–3876.
(23) Buchin, B.; Gemel, C.; Kempter, A.; Cadenbach, T.; Fischer, R. A. *Inorg. Chim. Acta* **2006**, *359*, 4833–4839.
(24) Cadenbach, T.; Gemel, C.; Zacher, D.; Fischer, R. A. *Angew. Chem., Int. Ed.* **2008**, *47*, 3438–3441.
(25) Gemel, C.; Steinke, T.; Weiss, D.; Cokoja, M.; Winter, M.; Fischer, R. A. *Organometallics* **2003**, *22*, 2705–2710.

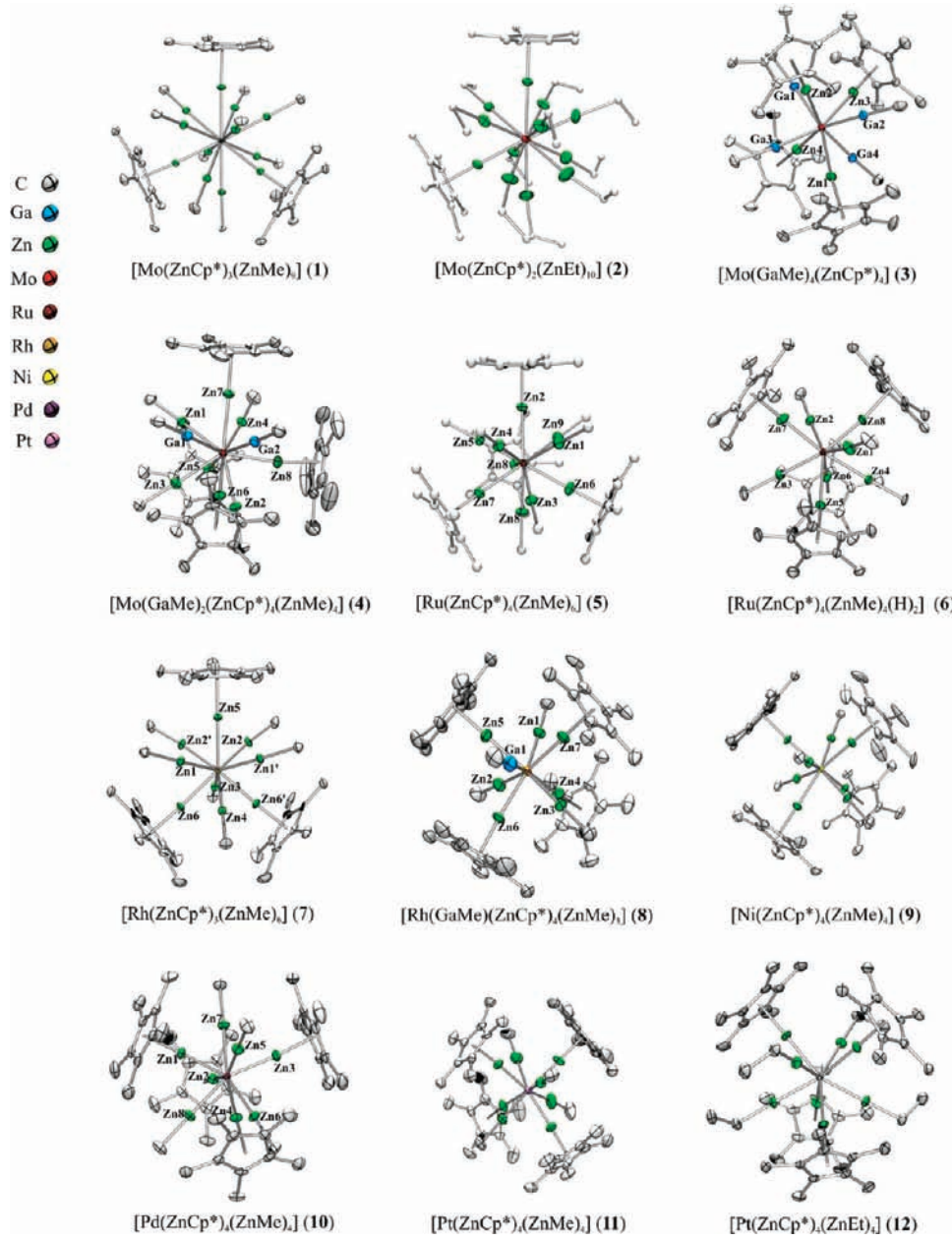

Figure 2. Molecular structures of **1**−**12** determined by X-ray single crystal diffraction. Important structural data on the metal−metal bonding are compiled in Table 2. Further details on the X-ray data collection and structure determination and refinement are given in Table S1 of the Supporting Information. The Ga/Zn assignement shown in the structure of **4** is one of three alternatives derived from ^{1}H NMR spectroscopy. A precise assignment is not possible based on the available analytical data.

All reported compounds **1**−**12** fulfill the classic 18-electron rule in coordination chemistry.[26] The compliancy of the 18-electron rule is evident from the formal valence electron count of the transition metal center, the treatment of the ZnR groups as 1 electron ligands and the GaR groups as 2 electron ligands. The synthesis of **1**−**12** involves the reduction of Zn(II) and a concomitant oxidation of Ga(I). The corresponding byproduct are Me_2GaCp^* (major) and other related organo Ga(III) species. The driving force of the reaction is certainly connected with the thermodynamically favorable oxidation of Ga(I) to Ga(III) combined with the very similar electronic and steric properties of the monovalent GaR and ZnR ligands at a transition metal center. We want to point out that the assignment of formal oxidation states to the ligand atoms Zn and Ga and the central transition metal in the new compounds is somewhat arbitrary (see below).

We neither observed elemental gallium or zinc nor other metallic deposits as byproduct. We do not have any data as of yet on mechanistic details, for example, evidence for free radicals or other reactive intermediates. Nevertheless, it is obvious that in the course of the overall redox-reaction, the resulting monovalent zinc fragments, ZnMe, ZnEt and ZnCp* are efficiently trapped by binding to the transition metal center resulting in rather strong covalent M−Zn bonds. Hence, the formal substitution of one GaR ligand always gives two ZnR ligands attached to the transition metal center. Consequently, the electron count of the product compounds do not change with the present amount of zinc in the ligand sphere and must sum

(26) Pyykkö, P. *J. Organomet. Chem.* **2006**, *691*, 4336–4340.

Table 2. Experimental Metal−metal Bond Lengths in Å[a]

M	metal core (compound number)	M−ZnCp*	M−ZnMe	M−GaMe	Ga/Zn−Zn
Mo	$MoZn_{12}$ (**1**)	2.672(1)−2.677(1)	2.636(1)−2.648(1)	−	2.724(2)−2.853(1)
		2.666−2.667	*2.673−2.678*		*2.796−2.832*
	$MoZn_{12}$ (**2**)	2.653(1)−2.657(2)	2.626(1)−2.684(2)	−	2.708(2)−2.833(2)
	$MoGa_4Zn_4$ (**3**)	2.528(2)−2.551(2)	−	2.385(2)−2.406(2)	2.778(2)−3.014(2)
		2.588−2.590		*2.426−2.427*	*2.880−2.932*
	$MoGa_2Zn_8$ (**4**)	2.616(1)−2.635(1)	2.469(1)−2.577(1)	2.488(1)−2.579(1)	2.738(1)−3.024(1)
		2.622−2.646	*2.628−2.647*	*2.450−2.457*	*2.729−3.053*
Ru	$RuZn_{10}$ (**5**)	2.545(1)−2.567(1)	2.489(1)−2.503(1)	−	2.676(1)−2.983(1)
		2.554−2.564	*2.524−2.544*		*2.723−3.036*
	$RuZn_8$ (**6**)	2.469(1)−2.488(1)	2.438(1)−2.492(1)	−	2.722(1)−3.147(1)
Rh	$RhZn_9$ (**7**)	2.471(2)−2.503(2)	2.439(2)−2.470(3)	−	2.749(2)−2.990(2)
		2.506−2.508	*2.488−2.490*		*2.850−2.995*
	$RhGaZn_7$ (**8**)	2.432(1)−2.439(1)	2.394(1)−2.398(1)	2.384(1)	2.814(1)−3.052(1)
		2.476−2.493	*2.468*	*2.309*	*2.850−2.942*
Ni	$NiZn_8$ (**9**)	2.351(1)−2.371(1)	2.313(1)−2.330(1)	−	2.746(1)−2.912(1)
		2.380	*2.357*		*2.772−2.836*
	$PdZn_8$ (**10**)	2.447(1)−2.459(1)	2.417(1)−2.424(1)	−	2.824(1)−3.133(1)
		2.492−2.493	*2.458−2.459*		*2.866−2.953*
Pt	$PtZn_8$ (**11**)	2.441(1)−2.459(1)	2.402(1)−2.467(1)	−	2.812(2)−3.115(2)
		2.506−2.508	*2.476−2.477*		*2.888−2.956*
	$PtZn_8$ (**12**)	2.457(1)−2.459(1)	2.425(1)−2.430(0)	−	2.842(1)−3.057(1)

[a] Respective calculated bond lengths of model compounds where Cp* is replaced by Cp are given in *italics*.

up to 18 electrons in all cases. The total and always even number of Zn ligands in the complexes is only dependent on the number of gallium ligands in the precursor as well as the amount of $ZnMe_2$ used in the reaction. Thus, treatment of the precursors [M(GaCp*)$_n$] with an excess $ZnR_2 > 2n$ leads to the pseudo homoleptic compounds [M(ZnCp*)$_a$(ZnR)$_b$] ($a + b = 2n$). Since the Cp* and the alkyl substituents R at gallium and zinc are known to be fluxional and/or transferable[11,24] a further rise in the excess of ZnR_2 is likely to allow the formation of truly homoleptic compounds of the type [M(ZnR)$_n$] in case of a quantitative exchange of Cp* against R (see the compositions of compounds **1** and **2**).

It is not ruled out with certainty, that synthesis of compounds similar to **1**−**12** and even going left in the periodic table beyond group 6 may be possible by circumventing the apparent bottleneck of quite exotic precursors like **13**−**18** in some way. However, success in obtaining **1**−**12** directly from commercially available transition metal halides MX_n or carbonyls $M(CO)_n$ etc. in the presence of ZnR_2 and other additional reducing agents is highly unlikely (at least we have failed so far). The unique combination of several features of the carbenoid GaCp* ligand appears to be quite important for the efficiency of the reported synthesis. GaCp* strongly stabilizes the low and even zero oxidation states of transition metals, it acts as a very powerful but selective reducing agent and bears the coordinative flexible Cp*-ligand which can be regarded as a transferable protecting group between metal atoms.

1.1. Molybdenum Compounds. The new homoleptic complex [Mo(GaCp*)$_6$] (**13**)[16,21] is the precursor of choice for the synthesis of **1**−**4**. This particular compound is so far the only homoleptic *and* heteroatom-free all-gallium coordinated metal complex with a coordination number of six. Note that the related complex [Ru(GaCp*)$_6$Cl$_2$] (**15**) bears two Ga-bridging Cl-ligands in the periphery.[23] Only two other neutral and mononuclear group-13 metal (E) transition metal (M) complexes with coordination number >4 are known. They exhibit the formal composition ME_5, that is, M(AlCp*)$_5$ (M = Fe, Ru), but the molecular structure of these complexes differs from the simple situation suggested by the composition and involves C−H activation of the peripheral C−H bonds of the Cp* substituents.[27] When compound **13** is treated with a 14-fold molar excess of $ZnMe_2$ in toluene at 110 °C for a period of over 2 h, compound [Mo(ZnMe)$_9$(ZnCp*)$_3$] (**1**) is formed quantitatively as judged by NMR (Scheme 1, Figures 1, 2). It crystallizes in big yellow prismatic single crystals in a very good preparative yield of 80−90% when the solution is cooled to room temperature. The molecular structure of **1** shows almost perfect icosahedral environment of the Mo atom by 12 ZnR ligands with a distribution of 9 methyl and 3 Cp* substituents in such a way that the η^5-coordinated, bulky Cp* groups occupy positions as far from each other as possible, resulting in an overall C_3 symmetry.

The structural and spectroscopic features of **1** were presented and discussed in detail in our previous communication and are not repeated herein.[16] Raising the excess of $ZnMe_2$ and prolonging the heating did not further change the product, that is, we did not succeed in deriving the fully homoleptic parent compound [Mo(ZnMe)$_{12}$] in a pure form. However, by using $ZnEt_2$ instead of $ZnMe_2$, we isolated the related compound [Mo(ZnEt)$_{10}$(ZnCp*)$_2$] (**2**) in good yields. The solution ^{1}H NMR spectra of the isolated crystals of **2** in C_6D_6 at room temperature and at 80 °C are very complicated, presumably showing several isomers and thus cannot be fully assigned (see Experimental Section for details). A fast interconversion of these isomers at 80 °C can be excluded based on these results. One of the isomers of **2** with the Cp*Zn units in the "*meta*" position (Figure 2) was obtained in a pure form by crystallization from the reaction solution and subsequent crystal picking. The structural features (i.e. Mo−ZnR and Zn−Zn bond lengths), are almost identical to those of **1** (see Table 2) and are thus not discussed further. This result at least points to the possible stability of homoleptic [Mo(ZnR)$_{12}$], which might be accessible under the proper conditions including the choice of R. Apparently, the use of steric slightly more demanding ZnEt groups leads to less ZnCp* groups in the product.

Interestingly, by reducing the amount of $ZnMe_2$ but leaving the other conditions unchanged, the two Zn/Ga mixed ligand

(27) Steinke, T.; Cokoja, M.; Gemel, C.; Kempter, A.; Krapp, A.; Frenking, G.; Zenneck, U.; Fischer, R. A. *Angew. Chem., Int. Ed.* **2005**, *44*, 2943–2946.

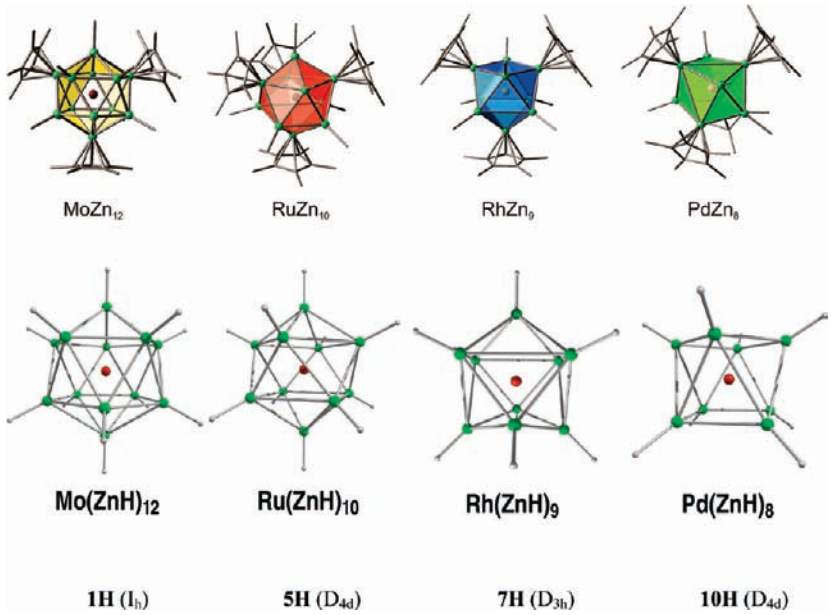

Figure 3. Molecular structures of **1**, **5**, **7** and **10** showing the coordination polyhedron around the central metal M and the corresponding parent molecules $[M(ZnH)_n]$ (**1H**, **5H**, **7H** and **10H** used for the quantum chemical calculations).

complexes $[Mo(GaMe)_4(ZnCp^*)_4]$ (**3**) and $[Mo(GaMe)_2(ZnCp^*)_4(ZnMe)_4]$ (**4**) were isolated, which can themselves be converted to **1** quantitatively by subsequent treatment with excess of $ZnMe_2$. Thus, the compounds **3**-**4** are intermediates of the formation of **1** (Scheme 1). Taking into account that the ^{1}H NMR spectrum of pure **3** in C_6D_6 reveals two sharps signals at $\delta = 2.07$ and 0.39 ppm, two isomers of **3** with exchange of the Cp* vs Me between the Ga and the Zn atoms are possible, that is, $[Mo(GaMe)_4(ZnCp^*)_4]$ and $[Mo(GaCp^*)_4(ZnMe)_4]$. The isomer with the Cp* groups bonded to the Zn center, $[Mo(GaMe)_4(ZnCp^*)_4]$, is favored by 20 kcal/mol as shown by DFT calculations (see below and the Supporting Information Figure S6). On the basis of this result, we give preference to ZnCp* over GaCp* and GaMe over ZnMe when choosing for the refinement of all crystal structures of the mixed Ga/Zn complexes **3**−**4** and **8**.

The molecular structure of **3** (Figure 2, important crystallographic data are summarized in Supporting Information Table S1) reveals the Mo center coordinated by four GaMe and four ZnCp* ligands. Again, the η^5-Cp* groups occupy positions as far as possible from each other resulting in superimposed Zn_4 and Ga_4 tetrahedra. This gives an overall, yet slightly distorted trigonal dodecahedral structure (eight vertices, twelve triangular planes, see the structure of **10H** in Figure 3, below). The structure is closer to a dodecahedron than to a square antiprism, showing Ga_2Zn_2 torsion angles of 20.94° for Ga(1)−Zn(2)−Ga(2)−Zn(3) and 30.28° for Ga(3)−Zn(1)−Ga(4)−Zn(4). The Mo−ZnCp* distances are between 2.528(2)−2.551(2) Å and are substantially shorter than those in $[Mo(ZnCp^*)_3(ZnMe)_9]$ (**2**) (2.672(8)−2.677(13) Å) or $[\{Mo(CO)_4\}_4(Zn)_6(\mu\text{-}ZnCp^*)_4]$ (2.664(1)−2.681(1) Å), which is presumably a consequence of the decreased coordination number of the molybdenum atom. Only few examples of organometallic transition metal Zn complexes are known.[13] Typical distances of Mo−Zn bonds are between 2.538(1)−2.793(3) Å.[13p,q] The Mo−GaMe distances tend to be shorter and range from 2.385(2) to 2.406(2) Å with an average value of 2.396 Å whereas the Ga−Zn distances in the Ga_4Zn_4 metal sphere are between 2.778(2) and 3.014(2) Å. These latter values do not rule out weak metal−metal bonding. Typical Ga−Zn distances in intermetallic compounds range between 2.75 and 3.00 Å.[15]

By use of eight molar equivalents of $ZnMe_2$ the second intermediate, namely $[Mo(ZnCp^*)_4(ZnMe)_4(GaMe)_2]$ (**4**) was isolated in high yields (see Scheme 1). Compound **4** is also obtained when **3** was treated with four molar equivalents of $ZnMe_2$, suggesting consecutive formation of the two intermediates **3** and **4** in the direct synthesis of **1**. The Zn_8Ga_2 coordination sphere of **4** (Figure 2, Table S1) represents a distorted bicapped square antiprism resulting in torsion angles of 0.07° for Zn(1)−Ga(1)−Ga(2)−Zn(4) and 11.37° for Zn(5)−Zn(3)−Zn(6)−Zn(8) as well as an Zn(6)−Ga(2)−Ga(1) angle of 59.79(3)°. The two capping ligands ZnCp* and ZnMe are in a *trans* position and are slightly bent toward each other resulting in an Zn(2)−Mo(1)−Zn(7) angle of 161.88(4)°. Due to the higher coordination number of the Mo center in **4** with respect to **3**, the Mo−ZnCp* as well as the Mo−GaMe bond lengths in **4** are significantly longer than those in **3** (see Table 2). Interestingly, the metal−metal distances in the Ga_2Zn_8 cage remain almost unchanged (2.738(1) - 3.024(1) Å). The ^{1}H NMR spectrum of **4** at room temperature exhibits three signals at $\delta = 2.14$ (30H), 2.07 (15H) and 1.91 ppm (15H) which are assigned to the Cp* groups. In addition, the spectrum displays one signal for both GaMe units at $\delta = 0.56$ ppm (6H) and three signals for the four ZnMe fragments at $\delta = 0.14$ (3H), 0.02 (6H) and −0.01 ppm (3H). Due to the low solubility of **4** no ^{13}C spectrum could be obtained. At 70 °C the ^{1}H NMR spectrum shows a fluxional behavior leading to one Cp* signal at $\delta = 2.09$ ppm and one signal for the ZnMe groups at $\delta = -0.03$ ppm while the signal for the GaMe units remains unchanged. These experiments are consistent with the symmetry resulting from the assignment for the Ga/Zn positions in the solid state structure (Figure 2). It should be noted that **4** is the only example of compounds **1**−**12** showing fluxional behavior at the NMR time scale.

1.2. Ruthenium Compounds. In analogy to the synthesis of **1**−**2**, treatment of $[Ru_2(Ga)(GaCp^*)_7(H)_3]$ (**14**)[22] with 22 mol equiv of $ZnMe_2$ in toluene at 80 °C cleanly leads to the pseudo homoleptic all zinc coordinated $[Ru(ZnCp^*)_4(ZnMe)_6]$ (**5**) in a

yield of 72% (see Scheme 1). Complex **5** is also accessible in lower yields by reaction of [Ru(GaCp*)$_6$(Cl)$_2$] (**15**)[23] with 20 mol equiv of $ZnMe_2$. The ^{1}H and ^{13}C NMR spectra are in good agreement with the solid state structure (*vide infra*) of idealized C_3 symmetry. The ^{1}H NMR signals for the Cp* and methyl groups are at δ = 2.07 (60H) and −0.19 ppm (18H) and the ^{13}C NMR resonances are at δ = 110.6 (C_5Me_5), 14.6 (CH_3) and 10.6 ppm ($C_5\mathit{Me}_5$). The absence of hydride ligands was confirmed by ^{1}H NMR-spectroscopy. The ruthenium center is coordinated by four ZnCp* and six ZnMe moieties, which leads to a deca-coordination (Figure 2, Table S1). Similar to [Mo(ZnCp*)$_4$(ZnMe)$_4$(GaMe)$_2$] (**4**), compound **5** adopts a slightly distorted bicapped square antiprismatic ligand environment (D_{4d}) with torsion angles of 0.42° for Zn(1)−Zn(4)−Zn(5)−Zn(9) and 9.04° for Zn(3)−Zn(6)−Zn(10)−Zn(7) as well as a Zn(4)−Zn(1)−Zn(3) angle of 59.90(3)°. The capping ligands ZnCp* and ZnMe are in a trans position and are slightly bent toward each other giving an angle Zn(8)−Ru(1)−Zn(2) of 159.36(4)°. The terminal Ru−ZnR distances range from 2.489(1) to 2.567(1) Å. These distances are distinctly shorter with respect to the bridging ZnEt units in the molecular compounds [{(η^5-C_5Me_5)Ru}$_3$(μ_3-ZnEt)(μ-H)$_3$(μ_3−H)] (2.6749(10) and 2.6562(8) Å) and [{(η^5-C_5Me_5)Ru}$_3$(μ_3-ZnEt)$_2$(μ-H)$_3$] (2.6414(10) Å).[131,m] The Ru−Zn bonds of **5** compare well with the situation in Ru/Zn solid state phases such as $RuZn_3$, for example, which however contains distorted $RuZn_{12}$ cuboctahedra with somewhat longer Ru−Zn distances of 262.49(4) and 279.12(4).[28]

Interestingly, by reducing the amount of $ZnMe_2$ to 16 mol equiv. the intermediate [Ru(ZnCp*)$_4$(ZnMe)$_4$(H)$_2$] (**6**) was isolated in good yields (Scheme 1). The ^{1}H NMR spectra of compound **6** at room temperature in C_6D_6 displays three sharp singlets at δ 2.00, −0.11, and −15.89 ppm with an integral ratio of 60:12:2 representing the four ZnCp* and ZnMe groups as well as two ruthenium bonded hydride ligands, which is consistent with an overall pseudo-T_d symmetry of the coordination polyhedron around the ruthenium center. The shift of the hydride signal is well in agreement with terminal Ru−H complexes reported in literature.[29] Down to −100 °C in toluene-d^8 the line-shapes and the chemical shifts of these signals do not change. In addition, the transversal relaxation time T1 for the hydride signal in **6** has been determined to be ≥300 ms, which clearly points to a classic dihydride structure rather than a dihydrogen complex.[30] Although the exact positions of the hydrides in the solid state structure of **6** cannot be located and refined, the presence of terminal Ru−H motifs in the solid state is further substantiated by IR spectroscopy which reveals two sharp absorptions in the expected region for terminal ruthenium hydride ligands (1923 and 1901 cm^{-1}). This coexistence of the ZnR ligands with the hydride ligands in the coordination sphere of ruthenium compares with the structures of the above-mentioned binuclear ZnEt bridged ruthenium clusters[13m,l] and directly underlines the analogous binding properties of terminal H and ZnR already mentioned in the introduction. As for the octa-coordinated **3**, the molecular structure of **6** (Figure 2, Table S1) shows an alternation of the ZnMe and ZnCp* positions in the coordination sphere around the ruthenium center minimizing steric interactions. Disregarding the hydrides, the pure metal cage shows a distorted dodecahedral environment with torsion angles of 39.30° for Zn(1)−Zn(7)−Zn(2)−Zn(8) and 29.60° for Zn(3)−Zn(5)−Zn(4)−Zn(6). The Ru−ZnCp* and the Ru−ZnMe bond distances are substantially shortened with respect to **5** (see Table 2) and the Zn−Zn distances are elongated accordingly.

1.3. Rhodium Compounds. The all-gallium penta-coordinated complex [(Cp*Ga)$_4$Rh(η^1-Cp*GaCH$_3$)][24] is the precursor of choice for the synthesis of the homoleptic rhodium congener to the above molybdenum and ruthenium compounds **1**−**2** and **5**. If [(Cp*Ga)$_4$Rh(η^1-Cp*GaCH$_3$)] is treated with 11 molar equivalents of $ZnMe_2$ in toluene at 110 °C over a period of 1 h the nona-coordinated [Rh(ZnCp*)$_3$(ZnMe)$_6$] (**7**) is obtained in good yield. An octa-coordinated Ga/Zn mixed compound [Rh(GaMe)(ZnCp*)$_4$(ZnMe)$_3$] (**8**) related to the mixed Ga/Zn compounds **3**−**4** is obtained in almost quantitative yields as an intermediate of this reaction by using seven instead of eleven molar equivalents of $ZnMe_2$ (see Scheme 1). Single crystals of **7** suitable for X-ray diffraction studies were grown as described for the previous cases (Table S1). The determined molecular structure reveals a quite perfect single capped square antiprismatic coordination environment of the Rh atom by nine ZnR ligands with a distribution of six methyl and three Cp* substituents in such a way, that again the bulky η^5-Cp* groups occupy positions as far as possible from each other resulting in an overall C_3 symmetry (Figure 2). Almost perfect torsion angles for the respective Zn planes of nearly 0° and a Zn1−Zn1′−Zn4 angle of 56.76° are found. The capping ligand ZnCp* is located directly above the center of the Zn1−Zn1′−Zn2−Zn2′ plane with an angle Rh−Zn5-(Zn1−Zn1′−Zn2−Zn2′)$_{centroid}$ of 174.26°. The Rh−Zn distances are almost equal with 2.471(2)−2.503(2) Å for Rh−ZnCp* and 2.439(2)−2.470(3) Å for Rh−ZnMe. The Zn−Zn distances in the Zn_9 polyhedron are between 2.749(2) and 2.990(2) Å. Only two examples of Rh−ZnR complexes are known, however only with bridging Rh−Zn−Rh moieties. The respective Rh−Zn bond distances are 2.558(1) and 2.513(1) Å in [{({Pr$^i_2$P(CH$_2$)$_3$PPr$^i_2$)Rh}$_2$(μ-H)$_2$(μ-ZnCH$_2$Ph)$_2$][13j] and 2.453(1)− 2.6115(8) Å in [{(dippp)Rh}$_2$(μ-H)$_2$(μ-ZnC$_5$H$_5$)$_2$].[13k] The ^{1}H and ^{13}C NMR spectra of **7** in solution agree with the solid state structure and display chemically equivalent Cp* and methyl groups. The molecular structure of **8** (Figure 2, Table S1) is very similar to the other octa coordinated complex **3**,that is, the eight ligands around the transition metal center define a slightly distorted trigonal dodecahedron rather than a square antiprism (*vide supra*). The torsion angles of the Zn(1)−Zn(5)−Ga(1)−Zn(7) and the Zn(4)−Zn(2)−Zn(6)−Zn(3) are 19.62 and 20.51°, respectively, whereas the Zn(7)−Zn(3)−Ga(1) angle is 58.46(2)°. It should be noted that two different isomers are observed in the ^{1}H NMR spectra of **8**, which show no line broadening up to 70 °C pointing to interconversion processes at this temperature (see experimental section for details).

1.4. Nickel, Palladium and Platinum Compounds. Reaction of the homoleptic complexes [M(GaCp*)$_4$] (M = Ni, Pd, Pt)[25] with 10 molar equivalents of $ZnMe_2$ in toluene at 80 °C very cleanly lead to the expected all zinc containing complexes [M(ZnCp*)$_4$(ZnMe)$_4$] with M = Ni (**9**), Pd (**10**) and Pt (**11, 12**). Compounds **9**−**12** are isostructural with only the expected variations of the M−Zn and Zn−Zn distances. Only [Pd(ZnCp*)$_4$(ZnMe)$_4$] (**10**) (Figures 2, 3) is briefly discussed herein as the representative example of the full homologous series (all details are compiled in Table S1). As observed for the octa-coordinated **3** and **7** (*vide supra*) a slightly distorted trigonal dodecahedral environment is found for **10** rather than a square antiprism. The torsion angles are 21.37° for Zn(5)−Zn(3)−Zn(7)−Zn(1) and 20.15° for Zn(4)−Zn(6)−Zn(2)−Zn(8) and

(28) Allio, C.; Harbrecht, B. *Dalton Trans.* **2006**, 5352–5356.
(29) Sabo-Etienne, S.; Chaudret, B. *Mod. Coord. Chem* **2002**, *4*, 5–58.
(30) Hamilton, D. G.; Crabtree, R. H. *J. Am. Chem. Soc.* **1988**, *110*, 4126–4133.

an Zn(1)−Zn(5)−Zn(8) angle of 56.93°. Interestingly, the MZn_8 motif is also found in the solid state structures of M_1Zn_1 alloy phases (M = Ni, Pd, Pt), however, with square prismatic rather than antiprismatic coordination environment around the central M. The M−Zn distances in these solid state structures (2.525 Å for NiZn, 2.646 Å for PdZn and 2.68 Å for PtZn) are all considerably longer than in the respective complexes **9**, **10**, **11** and **12** (Table 2)[31] To the best of our knowledge, only one example of a covalent Pd−Zn bond has been reported in molecules, namely (^{F}PNP)Pd−Zn−Pd(PNP^F) (PNP^F = $(C_6H_3FP^iPr_2)_2N$), which expectedly shows slightly shorter Pd−Zn distances of 2.379(1) and 2.372(10) Å than those observed in **10**.[13o] The Zn−Zn distances in the Zn_8 cage range from 2.824(1) to 3.133(1) Å and are comparable to those of the other pseudo homoleptic complexes. The ^{1}H NMR spectrum of **10** is as expected and exhibits two signals at δ = 2.08 (ZnCp*) and 0.04 ppm (ZnMe) in the ratio of 60:12. The ^{13}C NMR spectrum does not exhibit any unusual feature. Finally it should be noted that reaction of [Pt(GaCp*)$_4$] with $ZnEt_2$ instead of $ZnMe_2$ lead to the analogous [Pt(ZnCp*)$_4$(ZnEt)$_4$] (**12**) which is isostructural to **11**.

2. Quantum Chemical Calculations and Analysis of the Bonding Situation. In view of the nontrivial bonding situation of the transition metal compounds which are reported here, we want to explain the terms which we are using for the different types of bonding. We distinguish between an electron sharing bond A−B where bond formation formally takes place between two open-shell fragments A and B which contribute with one electron each to the covalent bond and a donor−acceptor bond A−B where closed-shell fragments bind in a way which is best described using the familiar Dewar−Chatt−Duncanson (DCD) model of donation and back-donation. Furthermore, it is obvious that redox processes are involved in the reactions. For example, $ZnMe_2$ is clearly a Zn(II) compound but the bonding situation in [Mo(ZnCp*)$_3$(ZnMe)$_9$] (**1**) shows that six of the twelve valence electrons of the ZnR ligands are used for electron-sharing Mo−Zn bonds while six are used for delocalized Zn−Zn bonds (see below). Taking into account the rather different electronegativities (Pauling scale) of Mo (2.2) and Zn (1.7) formal oxidation states of −6 for Mo and +1.5 for Zn are derived. However, using Allred Rochow electronegativities with Mo (1.3) and Zn (1.7) a different result of +6 for Mo and +0.5 for Zn may be obtained. Obviously, a situation like this is ambiguous and it becomes especially complicated when the metal−ligand bonding comes from a mixture of donor−acceptor and electron sharing interactions and when GaR and ZnR ligands are involved (see Supporting Information). As is discussed below the calculations show that the central transition metal atom always carries a small negative charge between −0.1e and −0.2 e and the Zn atoms are slightly positively charged <+0.5e. We agree with one referee who argued that the oxidation state concept breaks down for our molecules. Thus, we will refrain from the assignment of formal oxidation states for the metal atoms in the compounds **1**-**12**. Rather, the bonding situation can be well described when the molecular orbitals are analyzed with charge and energy decomposition methods which shall be discussed in the following.

In our previous communication,[16] we found that the bonding situation in the $MoZn_{12}$ core of [Mo(ZnCp*)$_3$(ZnMe)$_9$] (**1**) is only slightly distorted from the bonding in the parent model compound [Mo(ZnH)$_{12}$] (**1H**) which has perfectly icosahedral (I_h) symmetry (Figure 3). The bonding analysis of **1H** using AIM and MO correlation diagrams suggested that the 18 valence electrons which are available for Mo−Zn and Zn−Zn bonding interactions yield six 2-electron-3-center Mo−Zn bonds (Figure 1) and three rather weak delocalized Zn−Zn bonds. It is noteworthy to mention that the AIM analysis gives twelve bond paths for the Mo−ZnH linkages but there is no Zn−Zn bond path in **1H**. The weak Zn−Zn bonds mainly serve to minimize ligand−ligand repulsion which enables the exceptional high coordination number as compared with usual transition metal complexes [ML_n] of *monodentate* ligands L. It was pointed out that icosahedral symmetry is perfectly suited for sd^5 hybridized metal orbitals because the shape of the sd^5 hybrids has twelve lobes which point into the corner of an icosahedron.[32] The question arises if the bonding situation in the other MZn_n cores where n = 8, 9, 10 may be interpreted in the same way as it was done for **1H**.

To analyze the bonding situation in the newly synthesized compounds shown in Table 1 we performed quantum chemical DFT calculations at the RI-BP86/def2-TZVPP and BP86/TZ2P+ levels of theory. First we optimized the geometries of **3**−**5** and **7**−**11** where we replaced Cp* by Cp. We did not calculate the parent compounds of **2** and **12** which carry ZnEt groups nor did we optimize the geometry of **6** which exhibits Ru−H bonds because they are not of immediate importance for the theoretical part of the work presented herein. A comparison of the calculated bond lengths of the MZn_n cores of the above parent compounds (Figure 3) with experimental data shows a very good agreement (Table 2). The rather small deviations between theory and experiment may be due to solid state effects. We then optimized the geometries of the model compounds [M(ZnH)$_n$] (**3H**−**5H** and **7H**−**11H**) where the Cp groups are substituted by H. The calculated bond lengths in the metal cores of these H substituted parent systems of the experimental compounds are very similar to the values of the calculated Cp substituted derivatives (see Table 2 and Table S2). It is thus justifiable to analyze the bonding situation in the H-substituted models [M(ZnH)$_n$] to explain the nature of the metal−ligand bonding in the experimental complexes which carry organic groups. Further on we discuss and compare the electronic structures of the model compounds [Mo(ZnH)$_{12}$] (**1H**), [Ru(ZnH)$_{10}$] (**5H**), [Rh(ZnH)$_9$] (**7H**) and [Pd(ZnH)$_8$] (**10H**) which are all shown in Figure 3. The geometry optimization of the latter species gave structures which have D_{4d} symmetry for **5H** and **10H** while **7H** has D_{3h} symmetry. The high symmetry of the homoleptic compounds makes it possible to analyze the metal−ligand orbital interactions in detail.

2.1. Bonding Situation in [Mo(ZnH)$_{12}$] (1H). The bonding situation in **5H**, **7H** and **10H** will be discussed in comparison with the parent molecule **1H**. Therefore we present a more detailed bonding analysis of **1H** than was given in our previous short communication.[16] In that work we showed that the three highest lying MOs are the triply degenerate $12t_{1u}$ orbital (HOMO), the quintuple degenerate 12 h_g orbital (HOMO-1) and the non degenerate $9a_g$ orbital (HOMO-2) which are shown in Figure 4. The $12t_{1u}$ orbital has negligibly small contributions

(31) (a) Heike, W.; Schramm, J.; Vaupel, O. *Metallwirtschaft, Metallwissenschaft, Metalltechnik* **1936**, *15*, 655–662. (b) Nowotny, H.; Bittner, H. *Monatsh. Chem.* **1950**, *81*, 679–680. (c) Nowotny, H.; Bauer, E.; Stempfl, A. *Monatsh. Chem.* **1950**, *81*, 1164–1164.

(32) (a) Tang, A. C. ; Lu, H. K. *J. Chin. Chem. Soc* **1950**, *17*, 251. (b) Tang, A. C. *J. Chin. Chem. Soc.* **1951**, *18*, 15. (c) Zhan, C.-G.; Liu, F.; Hu, Z.-M *Int. J. Quantum Chem.* **1987**, *32*, 13. For a pictorial representation of sd^n orbitals see: (d) Firman, T. K.; Landis, C. R. *J. Am. Chem. Soc.* **1998**, *120*, 12650.

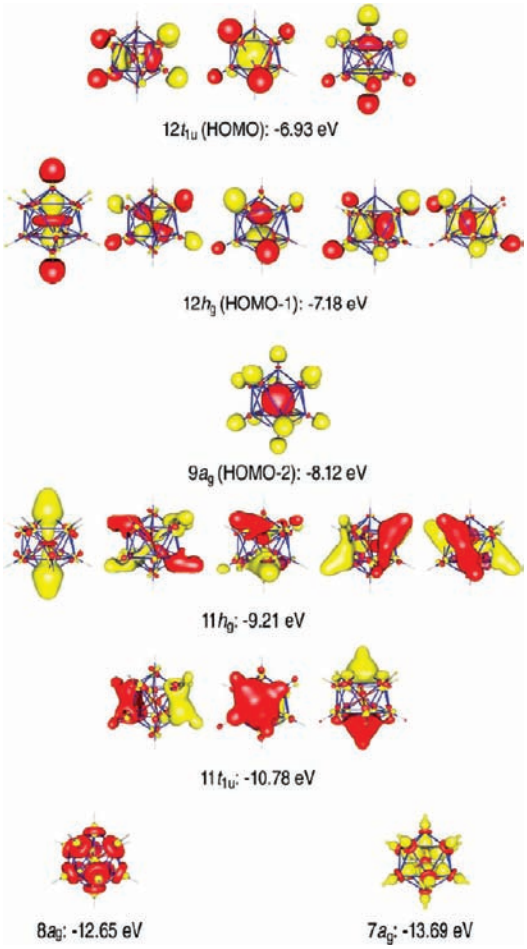

Figure 4. Molecular Orbitals of [Mo(ZnH)$_{12}$] (**1H**).

from the molybdenum 5p AOs while the 12 h_g orbital and the 9a_g orbital have large contributions from the molybdenum 4d and 5s AOs, respectively. There are a total of 81 occupied valence orbitals in [Mo(ZnH)$_{12}$]. The energy levels of the complete set of occupied valence orbitals of **1H** are shown in Figure S1 in the Supporting Information. Orbitals which belong to other irreducible representations of the I_h point group than the three which are mentioned above do not have contributions from the AOs of molybdenum. They describe occupied ligand orbitals of the (ZnH)$_{12}$ cage-like structure (but the zinc "cage" is instable without the central molybdenum atom). However, there are some lower-lying valence orbitals with t_{1u}, h_g and a_g symmetry than the above-mentioned frontier orbitals. They arise from the mixing of the (ZnH)$_{12}$ valence orbitals with the molybdenum valence AOs: three MOs which have a_g symmetry, five sets of MOs which have h_g symmetry and four sets of t_{1u} symmetry. Figure S1 also shows the lower lying occupied valence orbitals 11h_g, 11t_{1u}, 8a_g and 7a_g. The AO contributions of molybdenum in the remaining h_g and t_{1u} valence orbitals of **1H** are very small and therefore, they are not shown here. Visual inspection of the shapes of the orbitals shown in Figure 4 suggests that, besides the 12h_g (HOMO-1) set, the 11h_g orbitals should also contribute to the Mo−Zn bonding interactions while the effect of the 7a_g and 8a_g is difficult to assess. Like the 12t_{1u} HOMO, the 11t_{1u} orbital has only small contributions from the molybdenum 5p AOs which supports the statement that the orbitals with t_{1u} symmetry are mainly associated with Zn−Zn cage bonding. The strength of the overall contributions of the s, p and d orbitals of molybdenum to the Mo-(ZnH)$_{12}$ interactions can be quantitatively estimated with the EDA. Table 3 gives the numerical values of the calculations. It becomes obvious that the strongest orbital interactions come from the h_g orbitals which contribute 71.5% to ΔE_{Orb}. The latter is due to the bonding of the five d AOs of molybdenum which means that a single d(Mo) AO accounts for 14.3% of ΔE_{Orb} which is clearly less than the contribution of the s(Mo) AO (23.9%). The three valence p AOs of molybdenum add only 4.5% of the orbital interactions which is much less than the strength of the s(Mo) and d(Mo) AOs.

Table 3. EDA Results of [Mo(ZnH)12] at BP86/TZ2P[a]

ΔE_{int}	−348.8
ΔE_{Pauli}	594.5
ΔE_{elstat}[b]	−540.1 (57.2%)
ΔE_{Orb}[b]	−403.2 (42.8%)
$\Delta E_{Orb}(a_g)$[c]	−96.4 (23.9%)
$\Delta E_{Orb}(h_g)$[c]	−288.0 (71.5%)
$\Delta E_{Orb}(t_{1u})$[c]	−18.3 (4.5%)

[a] Interacting fragments are Mo(5s14d5) and (ZnH)12 with an electron configuration ag1hg5. Energy values in kcal/mol. [b] The percentage values in parentheses give the contribution to the total attractive interactions $\Delta E_{elstat}+\Delta E_{orb}$. [c] The percentage values in parentheses give the contribution to the total orbital interactions ΔE_{orb}

2.2. Bonding Situation in [Ru(ZnH)$_{10}$] (5H) in Comparison with [Mo(ZnH)$_{12}$] (1H). The equilibrium geometry of [Ru(ZnH)$_{10}$] (**5H**) has D_{4d} symmetry (Figure 3) which lifts the degeneracy of the MOs that involve the valence p and d orbitals of Ru. Molecular orbitals which have p(Ru) contributions have $b_2(p_z)$ or $e_1(p_x, p_y)$ symmetry while the MOs which comprise d(Ru) functions have $e_2(d_{xy}, d_{x^2-y^2})$, $e_3(d_{xz}, d_{yz})$ or $a_1(d_{z^2})$ symmetry. Note that the a_1 orbitals may also have contributions from the valence s(Ru) AO which have also a_1 symmetry. The EDA results can therefore not discriminate between the latter orbitals. The most important occupied valence orbitals of **5H** which have contributions from the ruthenium valence orbitals are shown in Figure 5. The energy levels of the complete set of 69 occupied valence orbitals of **5H** are shown in Figure S2 in Supporting Information. Visual inspection of the occupied MOs shown in Figure 5 indicates that the bonding pattern of the Ru−(ZnH)$_{10}$ interactions is similar to the Mo-(ZnH)$_{12}$ interactions in **1H** (Figure 4). The MOs 20e_1 (HOMO) and 20b_2 (HOMO-1) of **5H** are mainly cage orbitals with very small contributions from the p(Ru) AOs. They resemble the 12t_{1u}(HOMO) of **1H** (Figure 4). The orbitals 19e_3(HOMO-2), 18e_2(HOMO-3) and 21a_1(HOMO-4) of **5H** possess significant coefficients from the valence d(Ru) orbitals (Figure 5). They are related to the 12h_g (HOMO-1) orbital of **1H**. The next lower lying valence orbitals of **5H** which has large contributions from the d(Ru) AOs are 20a_1, 18e_3, 17e_2 and 19a_1 where the a_1 orbitals have large coefficients from the valence s(Ru) and d_{z^2}(Ru) AOs. The next lower lying orbitals of **5H** which have contributions from the valence p(Ru) AOs are the 19e_1 and 18b_2 MOs. These are also mainly cage orbitals with negligible coefficients at Ru. Further orbitals of **5H** exhibit large contributions from the valence s(Ru) and d(Ru) AOs. These are the 18a_1, 10e_2, 12e_3, 15a_1 and 14a_1 orbitals. The remaining occupied valence orbitals which have a_1, e_2 or e_3 symmetry show small coefficients at the Ru AOs. The energy decomposition analysis of **5H** is not as straightforward as the EDA of **1H** because the choice of the electronic states of the fragments for the Ru-(ZnH)$_{10}$ interactions is not clear-cut. We carried out the EDA calculations using different charges and electronic states of the fragments (numerical results see Table S3). The EDA data for Ru(ZnH)$_{10}$

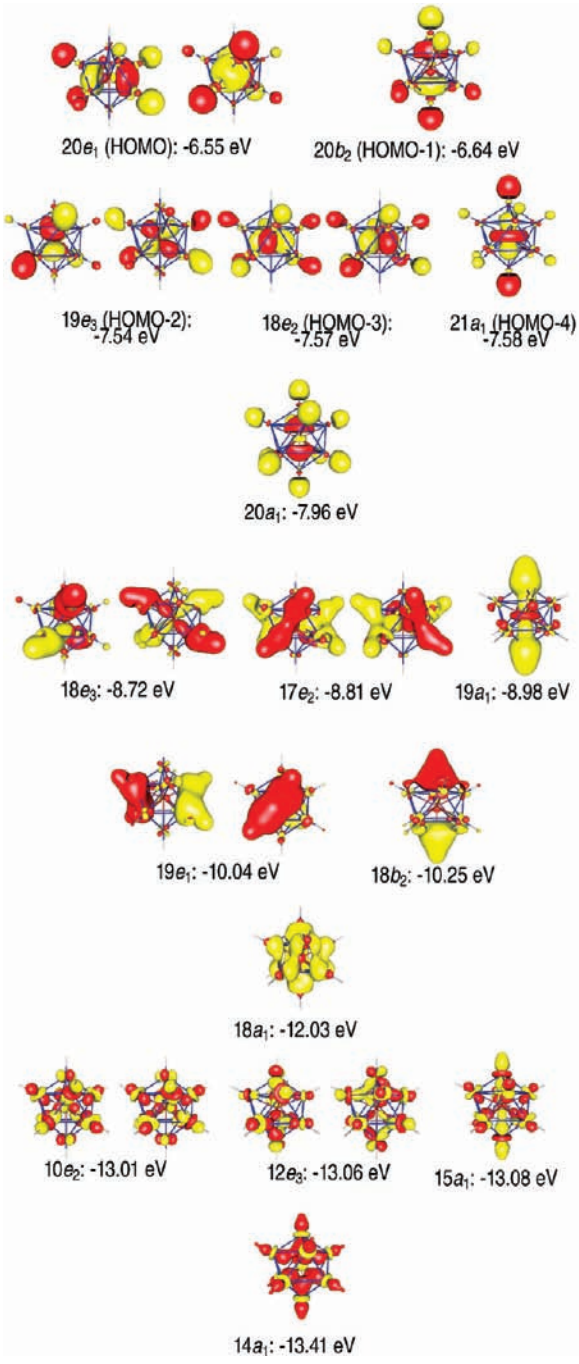

Figure 5. Molecular orbitals of $[Ru(ZnH)_{10}]$ (**5H**).

(**5H**) for the interaction of Ru^{2+} (s^1d^5) and $(ZnH)_{10}^{2-}$ in the septet states may be compared with the results for $Mo(ZnH)_{12}$ (**1H**) (Table S3) where the interacting fragments are the septet states of Mo (s^1d^5) and $(ZnH)_{12}$. It becomes obvious that the breakdown of the orbital term ΔE_{Orb} into the contributions from orbitals possessing different symmetry for **5H** gives a very similar result as for **1H**. The most important covalent bonding comes from the valence d orbitals of Ru. The contributions of the $(e_2)(d_{x^2-y^2},d_{xy})$ and $(e_3)(d_{xz},d_{yz})$ AOs comprise 64.6% of ΔE_{Orb}. It can be assumed that the d_{z^2} AO is as important as the other d-AOs of Ru. This means that the total orbital interaction of Ru in **5H** comes mainly from the valence d orbitals which account for 80.8% of ΔE_{Orb}. The contributions of the s(Ru) AO (8.8%) and the p(Ru) AOs (4.1%) are much smaller. The latter results may be biased by the choice of the charged fragments.

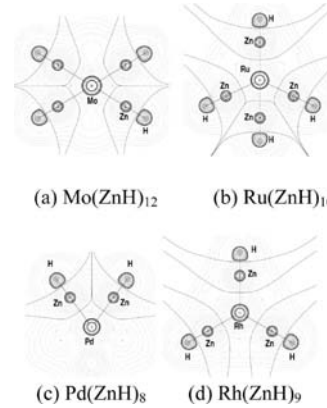

Figure 6. AIM calculations for (a) **1H**, (b) **5H**, (c) **10H** and (d) **7H** showing bond critical paths.

Table S3 gives also the EDA results where the interacting fragments $Ru(s^0d^8)$ and $(ZnH)_{10}$ are neutral species which are either in the triplet state or in the singlet state. If various charged fragments are chosen, the main differences between the obtained EDA data concern the relative contributions of the electrostatic bonding and the orbital interactions to the total attraction. Table S3 shows that about two-thirds of the attraction between Ru^{2+} and $(ZnH)_{10}^{2-}$ arises from ΔE_{Orb} and roughly one-third comes from ΔE_{elstat}. A reversed ratio is calculated for the interaction between the neutral fragments where ΔE_{elstat} is clearly stronger than ΔE_{Orb}. However, the breakdown of the latter term into orbitals having different symmetry supports the conclusions which come from the EDA results using charged fragments. The most important orbital interactions between the metal and the cage come from the d orbitals which account for roughly 80% of ΔE_{Orb}. Please note that the EDA results for the interactions between the triplet fragments give the smallest absolute value for ΔE_{Orb} which indicates that the best description for the Ru-$(ZnH)_{10}$ bonding is given in terms of the neutral triplet fragments $Ru(s^0d^8)$ and $(ZnH)_{10}$. This means that the Ru-$(ZnH)_{10}$ bonding involves electron-sharing interactions of the four unpaired electrons supported by donor−acceptor interactions between doubly occupied and vacant orbitals of Ru and $(ZnH)_{10}$. The calculated atomic partial charges at the Ru of −0.146e and at the Zn center of +0.176e supports the choice of neutral species as interacting fragments for the EDA of $M-(ZnH)_n$ bonding. Similar calculations were carried out for all model compounds **1H**, **3H**−**5H**, **7H**−**11H** and are compiled in Table S3−S5. The central transition metal atom always carries a small negative charge between −0.1e and −0.2 e except in $[Pd(ZnH)_8]$ (**10H**) where q(Pd) = +0.09e (see Table S6).

An intriguing result relating to the bonding situation in $Mo(ZnH)_{12}$ (**1H**) which we communicated previously[16] comes from the AIM calculations. Figure 6a shows that there are bond paths for the Mo−Zn and Zn−H interactions but there is no Zn−Zn bond path in **1H**. Figure 6b shows the Laplacian distribution, the bond paths and bond critical points and the zero-flux surfaces in the molecule plane of $Ru(ZnH)_{10}$ (**5H**). Like in **1H**, there are bond paths between the central transition metal atom and each Zn atom and there are Zn−H bond paths but there are no bond paths between the zinc atoms of the $(ZnH)_{10}$ cage. Note that the Zn−Zn distances in **5H** (2.740 Å and 2.798 Å) are even shorter than in **1H** (2.822 Å; Table 3). The bonding analyses suggest that $[Ru(ZnH)_{10}]$ exhibits multicenter Ru−Zn bonds that come from electron-sharing interac-

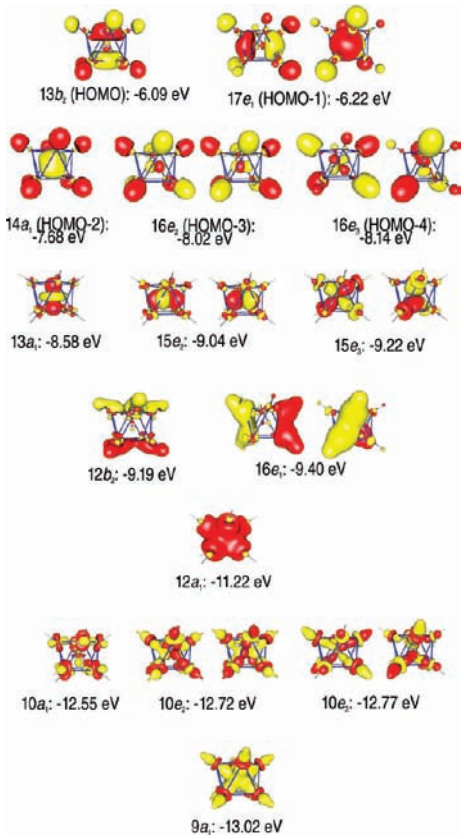

Figure 7. Molecular orbitals of [Pd(ZnH)$_8$] (**10H**).

tions as well as donor−acceptor interactions. The Zn−Zn interactions appear to be rather weak.

2.3. Bonding Situation in [Pd(ZnH)$_8$] (10H) and [Rh(ZnH)$_9$] (7H). The octa-coordinated model compound [Pd(ZnH)$_8$] **10H** has also D_{4d} symmetry (Figure 3). The Zn−Zn distances of the directly bonded zinc atoms in **10H** (2.936 Å and 3.149 Å) are clearly longer than in **1H** and **5H**. Thus it is not surprising that there are no Zn−Zn bond paths in the (ZnH)$_8$ polyhedron. There are only eight bond paths between Pd and the Zn atoms and there are eight Zn−H bond paths. Visual inspection of the valence MOs of [Pd(ZnH)$_8$] suggests a similar bonding situation as in **1H** and **5H**. The most important occupied valence orbitals of **10H** which have contributions from the palladium AOs are shown in Figure 7. The energy levels of the complete set of 57 occupied valence orbitals of **10H** are shown in Figure S3 in the Supporting Information.

The 13b$_2$(HOMO) and 17e$_1$(HOMO-1) are mainly cage orbitals with very small contributions from the p(Pd) AOs. They resemble the 12t$_{1u}$(HOMO) of **1H** (Figure 4). Below the HOMO and HOMO-1 there are ten orbitals which possess large coefficients from the valence s(Pd) and d(Pd) AOs. They can be grouped in sets of five orbitals which are close in energy. These are the 14a$_1$(HOMO-2), 16e$_2$(HOMO-3), and 16e$_3$(HOMO-4) orbitals (group 1) and the 13a$_1$, 15e$_2$, and 15e$_3$ orbitals (group 2). The next lower lying orbitals of **10H** with contributions from the valence p(Pd) AOs are the 12b$_2$ and 16e$_1$ MOs which are also mainly cage orbitals with negligible coefficients at Pd. The 12a$_1$ and 9a$_1$ MOs are lying below and have large coefficients at the valence s(Pd) AO. In between these latter orbitals is another set of five energetically close-lying MOs (10a$_1$, 10e$_2$, and 10e$_3$) with large coefficients from the valence d(Pd) AOs and thus, contribute to the total Pd-(ZnH)$_8$ orbital interactions.

The results of the EDA calculations for **10H** are reported in Table S4. The choice of the electronic states for the interacting fragments is straightforward because the ground state of Pd has a closed-shell s^0d^{10} configuration which is well suited for donor−acceptor interactions with the singlet state of (ZnH)$_8$. Note that the EDA results indicate that the Pd−(ZnH)$_8$ bonding comes mainly from electrostatic attraction (77.5% of ΔE_{int}) while only 22.5% of the total attraction comes from ΔE_{Orb}. The largest contribution to the latter term comes from the e$_2$(d_{xy}, $d_{x^2-y^2}$) and e$_3$(d_{xz}, d_{yz}) donation of Pd to the vacant orbitals of the (ZnH)$_8$ cage amount to 71.9% of the total orbital interactions. The orbital interactions of the a$_1$(s, d_{z^2}) orbitals gives only 16.0%, which means that the donation from the occupied cage orbitals into the s(Pd) AO appears to be small. Table S4 also gives the EDA results for the compounds of the other group-10 elements [Ni(ZnH)$_8$] (**9H**) and [Pt(ZnH)$_8$] (**11H**). The calculated values are very similar to those of [Pd(ZnH)$_8$] (**10H**).

The nona-coordinated compound [Rh(ZnH)$_9$] (**7H**) has D_{3h} symmetry (Figure 3). The Zn−Zn distances of the directly bonded zinc atoms (2.853 Å and 3.044 Å) are in the same range as in **10H**. Figure 6d shows that the AIM analysis gives no Zn−Zn bond paths while there are bond paths for the Mo−Zn and Zn−H pairs of atoms. Although **7H** has a lower symmetry than the other three model compounds discussed previously, it is possible to distinguish between the contributions of the different AOs of the central rhodium atom to the MOs. The bonding analysis including EDA is thus straightforward and results in quite a similar situation as presented for **1H**, **5H** and **10H**. The conclusion is that the most important orbital interactions in [Rh(ZnH)$_9$] come from the donation of the d(Rh) orbitals into the vacant cage orbitals of (ZnH)$_9$. The detailed discussion of the orbitals of **7H** is given in the Supporting Information (Figure S4, Table S5).

Discussion

From the viewpoint of coordination chemistry, the new compounds **1**-**12** are described as complexes [ML$_n$] (L = ZnR or GaR ligands) and are thus interesting in a 2-fold sense. First, they constitute an unprecedented series of unusual very zinc rich complexes with all zinc atoms binding to one single central transition metal. As a consequence of the fulfillment of the 18 electron rule, the resulting coordination numbers are very high and exceed the highest known coordination number of nine observed in molecular complexes for strictly monodentate, *non metal* ligator atoms L (e.g., or Nd(H$_2$O)$_9^{3+}$) and in particular for H as ligand which is isolobal to ZnR (i.e., ReH$_9^{2-}$). Note, that we rule out chelating ligands of any kind in this comparison.[33] Obviously, such high coordination numbers in [ML$_n$] molecules with L being an *arbitrary* ligand require an optimum balance between the radial M-L bonding interaction on the one hand and the tangential inter ligand interaction on the other hand. Steric crowding will prevent high coordination by repulsive interactions while substantial attractive interactions between the ligands or better to say between the ligator atoms will favor a cage molecule M@L$_n$ with the ligator atoms L forming a L-L bonded cage and *capture* the central metal M like in endohedral fullerenes M@C$_{60}$[34] or endohedral Zintl ions such as

(33) Ribas, G. J., *Coordination Chemistry*, 1st ed.; Wiley-VCH: Weinheim, 2008.
(34) Murata, M.; Murata, Y.; Komatsu, K. *Chem. Commun.* **2008**, 6083–6094.

$Pt@Pb_{12}^{2-}$.[35] However, in these cases, the radial interactions are weak and the captured interstitial metal does not contribute much to the overall stability of the cage. The bonding situation of the matrix species of composition WH_{12} cited in the introduction may be regarded as an example of these competing effects and the species is in fact a complex written as $[WH_4(H_2)_4]$. The systems $[M(ZnR)_n]$, with $[Mo(ZnCp^*)_3(ZnMe)_9]$ (**1**) being the key compound of the series, are clearly different from these highly coordinated metal hydride/hydrogen complexes. This concurs with the very different bond strengths of H_2 vs RZn−ZnR and of course with the highly unfavorable steric bulk of a side-on coordinated organo dizinc moiety rather than splitting this up into two very weakly interacting terminal ZnR units. Nevertheless, the H/ZnR isolobal analogy, which is particularly illustrated by compound **6** (Figure 2), is valid as a guideline for synthesis.

Looking at the analogy Au/ZnR or AuL/ZnR (L = phosphine, i.e. PPh_3, PEt_3) the structures and chemical bonding of **1**−**12** may alternatively be compared with naked or ligand stabilized endohedral gold clusters (neutral or charged species) of the general formula $M@Au_n$ or $M@(AuL)_n$ (L = alkyl/aryl phosphane). For example, **1** or **1H** are related to the gas-phase species MAu_{12} (M = Mo, W).[36] Autschbach et al.[37] discussed a closed-shell 18-electron bonding situation for the central tungsten atom with a significant population of the valence p orbitals. In addition, the relativistic aurophilic Au−Au interaction contributes substantially to the overall stability of the molecule and thus justifies the description as endohedral clusters $M@Au_{12}$. These latter details, however, are clearly different for **1H**. Zeng et al. performed a global search of highly stable endohedral gold clusters of the general formula $M@Au_n$ (n = 8−17) by DFT methods and found that the central metal M prefers to be entirely covered by gold for $n \geq 9$ and the clusters $M@Au_n$ exhibit large HOMO−LUMO gaps suggesting chemical stability, too.[38] Note, that the structures of the calculated species $Ru@Au_{10}$ (C_{2h}) and $Rh@Au_9$ (C_S) are very similar to $[Ru(ZnH)_{10}]$ (**5H**, D_{4d}) and $[Rh(ZnH)_9]$ (**7H**, D_{3h}) except for some differences in symmetry and corresponding details in the electronic properties.[38] But there are so far no structurally characterized and comparably close analogs for the series $[M(ZnH)_8]$ (M = Ni, Pd, Pt; **9H**−**11H**) and their experimental counterparts **9**−**12** in endohedral gold cluster chemistry. The well-known electronically unsaturated 16-electron clusters $[M(AuL)_8]^{2+}$ (M = Pd, Pt) exhibit quite different, ellipsoidal structures.[39] Addition of 2-electron Lewis base ligand result in nona-coordinated 18-electron spherical clusters, e.g. $[(CO)Pd(AuPPh_3)_8]^{2+}$.[40] The octa-coordinated neutral 18-electron cluster $[Pt(AuPPh_3)_8]$ is likely to have a similar structure to **11**−**12** and seems to be accessible by electrochemical reduction of $[Pt(AuPPh_3)_8]^{2+}$, but analytical details have not yet been published.[41] From these comparisons with homoleptic transition metal gold clusters it also follows, that even higher coordinated congeners of **1** might be a valid target for organometallic synthesis. The above cited calculations of Zeng et al. revealed particularly high binding energy per atom of $Zr@Au_{14}$, $Sc@Au_{15}$, and $Y@Au_{15}$.[38] In fact, preliminary calculations show that $[Zr(ZnH)_{14}]$ is a minimum on the potential energy surface and adopts Frank-Kasper polyhedral structure of D_{6d} symmetry (Figure S7). Analysis of the bonding in $[Zr(ZnH)_{14}]$ reveals an informative difference with regard to $[Mo(ZnH)_{12}]$ (**1H**). There are 14 bond paths for the Zr−Zn interactions. But now there are also Zn−Zn bond paths between the Zinc atoms of the planar Zn_6 moieties in $[Zr(ZnH)_{14}]$ which means *stronger* Zn−Zn bonding in the latter compound than in $[Mo(ZnH)_{12}]$. This is quite reasonable because in the latter compound there are six electron pairs for Mo−Zn bonding and only three electron pairs for Zn−Zn bonding while in $[Zr(ZnH)_{14}]$ there are only four electron pairs for Zr−Zn bonding and five electron pairs for Zn−Zn bonding. We thus speculate, that a stable compound of the type $[Zr(ZnR)_{14}]$ might be accessible if a suitable Zr precursor such as $[Zr(GaCp^*)_7]$ or other related compounds similar to the transition metal precursors **13**−**18** of Scheme 1 will be available sometime.

As we have pointed out in our previous communication,[16] we finally conclude that the key compound $[Mo(ZnCp^*)_3(ZnMe)_9]$ (**1**) is "chemically" best described as a perfectly sd^5 hybridized transition metal compound where all 12 lobes of the hybrid orbitals are used for strong covalent chemical bonding (Figure 1). The 18 valence electrons of **1** which are available for Mo−Zn and Zn−Zn bonding interactions yield six 2-electron-3-center Mo−Zn bonds and 3 very weak delocalized Zn−Zn bonds. The latter bonds just serve to minimize ligand−ligand repulsion and thus favor the exceptionally high coordination number as compared with usual transition metal complexes $[ML_n]$ of *monodentate* ligands L. The bonding situation of the other compounds **2**−**12** is more or less similar with deviations related to symmetry. This view of the bonding situation allows the comparison of these novel intermetallic molecules with main group non metallic "hypervalent" molecules, see, for example, SF_6, XeF_8 etc. as text book examples.[43]

Summary

In summary, the title compounds **1**−**12** represent a novel homologous series of molecules with quite a unique bonding situation which have been synthesized in substantial preparative quantities and structurally characterized by single crystal X-ray diffraction analysis. The organometallic fragments ZnR (R =CH_3, Et, Cp*) turn out to be surprisingly versatile by strongly binding to various transition metals as purely one electron donor ligands of tunable steric bulk without any substantial π-donor/acceptor properties. The high thermal stability of the new compounds together with the strict validity of the 18 electron rule suggests that the synthesis concept can be extended even further to many other metal atoms M of the periodic table which could be coordinatively saturated with ZnR groups. And vice versa, other unsaturated monovalent organo-metal fragments d^m−M′R (m = 0 or 10; M′ = Mg; Cd, Hg; Al, Ga, In; Sn, Pb

(35) Esenturk, E. N.; Fettinger, J.; Lam, Y.-F.; Eichhorn, B. *Angew. Chem., Int. Ed.* **2004**, *43*, 2132–2134.
(36) Li, X.; Kiran, B.; Li, J.; Zhai, H.; Wang, L. *Angew. Chem., Int. Ed.* **2002**, *41*, 4786–4789.
(37) Autschbach, J.; Hess, B. A.; Johansson, M. P.; Neugebauer, J.; Patzschke, M.; Pyykkö, P.; Reiher, M.; Sundholm, D. *Phys. Chem. Chem. Phys.* **2004**, *6*, 11–22.
(38) Gao, Y.; Bulusu, S.; Zeng, X. C. *Chemphyschem* **2006**, *7*, 2275–2278.
(39) Ito, L. N.; Brian, J; Johnson, B. J.; Mueting, A. M.; Pignolet, L. H. *Inorg. Chem.* **1989**, *28*, 2026–2028.
(40) Ito, L. N.; Felicissimo, A. M. P.; Pignolet, L. H. *Inorg. Chem.* **1991**, *30*, 988–994.
(41) Vanderlinden, J. G. M.; Roelofsen, A. M.; Ipskamp, G. H. W. *Inorg. Chem.* **1989**, *28*, 967–970.
(42) (a) Cotton, F. A.; Wilkinson, G.; Murillo, C. A.; Bochmann, M. *Advanced Chemistry*, 6th ed.; Wiley: New York, 1999; p 9. (b) Cotton, F. A. *Q. Rev.* **1966**, *20*, 389–401.
(43) (a) Housecroft, C. E.; Sharpe, A. G. *Inorganic Chemistry*, 3rd ed.; Pearson Education Limited: Edinburgh Gate, Harlow, England, 2008. (b) Kutzelnigg, W. *Angew. Chem., Int. Ed.* **1984**, *23*, 272–295. (c) Schleyer, P. v. R. *Chem. Eng. News* **1984**, *62*, 4.

etc.), if their actual steric and bonding properties are comparable to ZnR, may act as one, two or three electron ligands and will possibly allow the synthesis of ternary systems such as $[M(ZnR)_a(M'R)_b]$ with the 18 electron rule as a guideline for stable compositions (compounds **2**, **3** and **8** are first examples of this series). Last, but not least, we suggest the new compounds as precursors for the respective zinc rich nanoalloys and extending the scope of established soft-chemical concepts of nanometallurgy.[9,10,44] A door has been opened into a new field of metal rich molecules beyond the Zintl-boarder[45] bridging the gap between coordination compounds and clusters and linking the chemistry and physics of molecular compounds with intermetallic phases in a new way.

Experimental Section

General Considerations. All manipulations were carried out in an atmosphere of purified argon using standard Schlenk and glovebox techniques. The solvents were dried using an mBraun Solvent Purification System. The final H_2O content in all solvents was checked by Karl Fischer titration and did not exceed 5 ppm. GaCp*, $[Mo(\eta^4\text{-}C_4H_6)_3]$, $[Ru_2(Ga)(GaCp^*)_7(H)_3]$, $[Ru(GaCp^*)_6(Cl)_2]$, $[(Cp^*Ga)_4Rh(\eta^1\text{-}Cp^*GaCH_3)]$ as well as the homoleptic $[M(GaCp^*)_4]$ (M = Ni, Pd Pt) were prepared according to literature methods. Elemental analyses of all compounds were performed at the Laboratory for Microanalytics of the University of Essen (EA 1110 CHNS-O Carlo Erba Instruments for C, H, N and AAS measurements on a Thermo Electron M-Series spectrometer for Zn, Ga). NMR spectra were recorded on a Bruker Advance DPX-250 spectrometer (^{1}H, 250.1 MHz; ^{13}C, 62.9 MHz) in C_6D_6 298 K unless otherwise stated. Chemical shifts are given relative to TMS and were referenced to the solvent resonances as internal standards. All crystal structures were measured on an Oxford Excalibur diffractometer. The structures were solved by direct methods using SHELXS-97 and refined against F^2 on all data by full-matrix least-squares with SHELXL-97. Details of the structure determinations of products **1**−**13** are given in Table S1 (see Supporting Information). The files CCDC-741214−741224 contain the supplementary crystallographic data for this paper. These data can be obtained free of charge from the Cambridge Crystallographic Data Centre: www.ccdc.cam.ac.uk/data_request/cif.

$[Mo(ZnMe)_9(ZnCp^*)_3]$ (1). A sample of $[Mo(GaCp^*)_6]$ (**13**) (0.300 g, 0.226 mmol), whose synthesis is described below, was dissolved in toluene (5 mL) and was treated with 1.58 mL of a 2 M $ZnMe_2$ solution in toluene at room temperature (14 equiv, 3.168 mmol). The reaction mixture was warmed to 100 °C for 2 h whereupon a yellow solution was formed. After cooling to room temperature the solution was filtered and the solvent was removed *in vacuo*. The crude product was redissolved in hexane. The product crystallized by slow cooling to −30 °C. Yield: 0.263 g (82%). ^{1}H NMR (C_6D_6, 25 °C): δ = 2.14 (45H, C_5Me_5), 0.24 (9H, Me), 0.19 (9H, ZnMe), 0.03 (9H, Me); ^{13}C NMR (C_6D_6, 25 °C): δ =113.71 (C_5Me_5), 23.82 (Me), 23.37 (Me), 22.19 (Me), 11.38 (C_5Me_5). Elemental Anal. Calcd for $C_{39}H_{72}Zn_{12}Mo$: C, 32.95; H, 5.10; Zn, 55.20; Mo, 6.75; found: C, 32.66; H, 5.44, Zn, 55.01; Mo, 6.44; no gallium was detected.

$[Mo(ZnCp^*)_2(ZnEt)_{10}]$ (2). Compound **2** was prepared analogously to **1** as described above by using 14 mol equiv $ZnEt_2$ instead of 14 mol equiv of $ZnMe_2$. Yield: 52% yellow crystals. Note that several isomers exist in the solution of the obtained yellow crystals which could not be separated satisfactorily on a preparative scale, so far. ^{1}H NMR (C_6D_6, 25 °C): δ = 2.21 (s, C_5Me_5), 2.19 (s, C_5Me_5), 2.15 (s, C_5Me_5), 2.12 (s, C_5Me_5), 1.65 (m), 1.52 (m), 1.27 (m), 1.03 (m), 0.89 (m), 0.72 (m), 0.51 (m); ^{13}C NMR (C_6D_6, 25 °C): δ =114.30 (s), 114.08 (s), 113.91 (s), 111.98 (s), 41.06 (s), 38.43 (s), 38.35 (s), 37.50 (s), 36.49 (s), 36.38 (s), 34.97 (s), 34.60 (s), 34.33 (s), 34.11 (s), 31.95 (s), 29.55 (s), 29.41 (s), 27.22 (s), 25.62 (s), 23.04 (s), 22.78 (s), 20.83 (s), 18.89 (s), 14.52 (s), 14.34 (s), 11.64 (s), 11.40 (s), 11.12 (s), 10.89 (s), 10.85 (s), 10.54 (s), 10.43 (s), 10.40 (s), 9.58 (s). Elemental Anal. Calcd for $C_{40}H_{80}Zn_{12}Mo$: C, 33.32; H, 5.59; Zn, 54.43; found: C, 33.11; H, 5.24, Zn, 54.28; no gallium was detected.

$[Mo(GaMe)_4(ZnCp^*)_4]$ (3). A sample of 13 (0.300 g, 0.226 mmol) was dissolved in toluene (5 mL) and treated with 0.45 mL of a 2 M $ZnMe_2$ solution in toluene at room temperature (4 eq, 0.904 mmol). The reaction mixture was warmed to 100 °C for 45 min whereupon a yellow solution was formed. After cooling to room temperature the solution was filtered and the solvent was removed *in vacuo*. The crude product was redissolved in hexane. The product crystallized by slowly cooling to −30 °C. Yield: 0.237 g (85%). ^{1}H NMR (C_6D_6, 25 °C): δ = 2.07 (s, 60H, C_5Me_5), 0.39 (s, 12H, Me); ^{13}C NMR (C_6D_6, 25 °C): δ = 109.75 (s, C_5Me_5), 34.10 (s, GaMe), 11.06 (s, C_5Me_5); Elemental Anal. Calc. for $C_{44}H_{72}Ga_4Zn_4Mo$: C, 42.71; H, 5.86; Ga, 22.54; Zn, 21.14; Mo, 7.75; found: C, 42.56; H, 5.82; Ga, 22.36; Zn, 21.25; Mo, 7.87.

$[Mo(GaMe)_2(ZnCp^*)_4(ZnMe)_4]$ (4). A sample of **13** (0.300 g, 0.226 mmol) in benzene (5 mL) was treated with 0.90 mL of a 2 M $ZnMe_2$ solution in toluene at room temperature (8 eq, 1.808 mmol). The reaction mixture was refluxed for 30 min whereupon a yellow microcrystalline precipitate was formed. The precipitate was isolated by means of decantation of the supernatant (cannula technique), washed twice with a small amount of hexane and dried *in vacuo*. The product was recrystallized from hot benzene by slowly cooling it down to room temperature. Yield: 0.261 g (83%). ^{1}H NMR (C_6D_6, 25 °C): δ = 2.15 (s, 30H, C_5Me_5), 2.07 (s, 15H, C_5Me_5) 1.91 (s, 15H, C_5Me_5), 0.57 (s, 6H, Me), 0.14 (s, 3H, Me), 0.02 (s, 6H, Me), −0.14 (s, 3H, Me). Elemental Anal. Calcd for $C_{46}H_{78}Ga_2Zn_8Mo$: C, 39.76; H, 5.66, Ga, 10.04; Zn, 37.64; found: C, 39.99; H, 5.94, Ga, 10.28; Zn 37.19.

$[Ru(ZnCp^*)_4(ZnMe)_6]$ (5). (a) A mixture of $[Ru_2(Ga)(GaCp^*)_7(H)_3]$ (**14**) (0.300 g, 0.175 mmol) and $ZnMe_2$ (1.93 mL of a 2 M toluene solution, 3.861 mmol) in toluene was refluxed for 45 min whereupon a yellow microcrystalline precipitate was formed. The precipitate was isolated by means of decantation of the supernatant (cannula technique), washed twice with a small amount of hexane and dried *in vacuo*. The product was recrystallized from hot toluene by being slowly cooled down to −30 °C. Yield: 0.349 g (72%). ^{1}H NMR (C_6D_6, 25 °C): δ = 2.07 (s, 60H, C_5Me_5), −0.19 (s, 18H, ZnMe); ^{13}C NMR (C_6D_6, 25 °C): δ = 110.56 (s, C_5Me_5), 14.56 (s, ZnMe), 10.64 (s, C_5Me_5). Elemental Anal. Calc. for $C_{46}H_{78}Zn_{10}Ru$: C, 39.86; H, 5.67, Zn, 47.18; found: C, 39.47; H, 5.61, Zn 47.67; no gallium was detected. (b) A freshly prepared sample of $[Ru(GaCp^*)_6(Cl)_2]$ (**15**) (0.250 g, 0.178 mmol) was dissolved in 6 mL toluene and treated with 1.78 mL of a 2 M $ZnMe_2$ solution in toluene at room temperature (20 eq, 3.567 mmol). The reaction mixture was refluxed for 45 min whereupon a yellow microcrystalline precipitate was formed. The precipitate was isolated by means of decantation of the supernatant (cannula technique), washed twice with a small amount of hexane and dried *in vacuo*. The product was recrystallized from hot toluene by being slowly cooled down to −30 °C. Yield: 0.204 g (59%). Elemental Anal. Calcd for $C_{46}H_{78}Zn_{10}Ru$: C, 39.86; H, 5.67, Zn, 47.18; found: C, 39.99; H, 5.94, Zn 47.11; no gallium was detected.

$[Ru(ZnCp^*)_4(ZnMe)_4(H)_2]$ (6). Compound **6** was prepared analogously to **5** as described above in route **5a** by using 16 mol equivalents of $ZnMe_2$ instead of 22 mol equivalents. Yield: 0.367 g (84%). ^{1}H NMR (C_6D_6, 25 °C): δ = 2.00 (s, 60H, C_5Me_5), −0.11 (s, 12H, ZnMe), −15.89 (s, 2H, Ru−H); ^{13}C NMR (C_6D_6, 25 °C): δ =110.80 (s, C_5Me_5), 13.41 (s, ZnMe), 10.88 (s, C_5Me_5). IR ν = 1923, 1901 cm^{-1} (vs, H) Elemental Anal. Calcd for $C_{44}H_{74}Zn_8Ru$: C, 43.06; H, 6.08; Zn, 42.63; found: C, 43.41; H, 6.11, Zn, 42.39

$[Rh(ZnCp^*)_3(ZnMe)_6]$ (7). A freshly prepared sample of $[(Cp^*Ga)_4Rh(\eta^1\text{-}Cp^*GaCH_3)]$ (**16**) (0.300 g, 0.253 mmol) was

(44) (a) Cable, R. E.; Schaak, R. E. *Chem. Mater.* **2007**, *19*, 4098–4104. (b) Cable, R. E.; Schaak, R. E. *Chem. Mater.* **2005**, *17*, 6835–6841.
(45) Fässler, T. F.; Hoffmann, S. D. *Angew. Chem., Int. Ed* **2004**, *43*, 6242–6248.

dissolved in 6 mL toluene and treated with 1.45 mL (11 mol eq) of a 2 M $ZnMe_2$ solution in toluene. The reaction mixture was stirred for 1 h at 80 °C. After removal of the solvent *in vacuo* the dark residue was washed with a small amount of cold *n*-hexane. Recrystallization from hexane (−30 °C overnight) gave yellow prisms. Yield: Yield: 0.250 g yellow crystals (80%). ^{1}H NMR (C_6D_6, 25 °C): δ = 2.07 (s, 45H, C_5Me_5), −0.04 (s, 18H, ZnMe); ^{13}C NMR (C_6D_6, 25 °C): δ =111.29 (s, C_5Me_5), 23.82 (d, ZnMe, ^2J(Rh−C) = 5.01 Hz,), 10.78 (s, C_5Me_5). Elemental Anal. Calcd for $C_{36}H_{63}Zn_9Rh$: C, 36.42; H, 5.35; Zn, 49.57; found: C, 36.53; H, 5.48, Zn, 49.48; no gallium was detected.

[Rh(GaMe)(ZnCp*)$_4$(ZnMe)$_3$] (8). A freshly prepared sample of [(Cp*Ga)$_4$Rh(η^1-Cp*GaCH$_3$)] (**16**) (0.280 g, 0.245 mmol) was dissolved in 6 mL toluene and treated with 0.86 mL (7 mol equiv) of a 2 M $ZnMe_2$ solution in toluene. The reaction mixture was stirred for 1 h at 80 °C. After removal of the solvent *in vacuo* the dark residue was washed with a small amount of cold *n*-hexane. Recrystallization from hexane (−30 °C overnight) gave yellow prisms. Yield: 0.223 g yellow crystals (74%). Isomer 1 (main isomer): ^{1}H NMR (C_6D_6, 25 °C): δ = 2.15 (s, 15H, C_5Me_5), 2.14 (s, 15H, C_5Me_5), 2.06 (s, 30H, C_5Me_5), 0.42 (s, 3H, GaMe), −0.11 (s, 9H, ZnMe). Isomer 2 (side isomer): ^{1}H NMR (C_6D_6, 25 °C): δ = 2.06 (s, 60H, C_5Me_5), −0.06 (s, 3H, GaMe), −0.17 (s, 9H, ZnMe). ^{13}C NMR (C_6D_6, 25 °C): δ =110.17 (s, C_5Me_5), 110.11 (s, C_5Me_5), 32.08 (d, Ga/ZnMe, ^2J(Rh−C) = 7.62 Hz), 31.98 (d, Ga/ZnMe, ^2J (Rh−C) = 4.32 Hz), 17.84 (d, Ga/ZnMe, ^2J(Rh−C) = 4.59 Hz), 17.37 (d, Ga/ZnMe, ^2J(Rh−C) = 5.77 Hz), 11.09 (s, C_5Me_5), 10.99 (s, C_5Me_5), 10.94 (C_5Me_5) Elemental Anal. Calcd for $C_{44}H_{72}GaZn_7Rh$: C, 42.92; H, 5.89; Ga, 5,66; Zn, 37.17; found: C, 42.71; H, 5.49, Ga, 5.35; Zn, 37.48.

[Ni(ZnCp*)$_4$(ZnMe)$_4$] (9). A freshly prepared sample of [Ni(GaCp*)$_4$] (0.510 g, 0.581 mmol) was dissolved in 6 mL toluene and treated with 2.90 mL of a 2 M $ZnMe_2$ solution in toluene (10 mol eq.). The reaction mixture was stirred for 1 h at 80 °C. After removal of the solvent *in vacuo* the dark residue was washed with a small amount of cold *n*-hexane. Recrystallization from toluene (−30 °C overnight) gave yellow prisms. Yield: 0.458 g yellow crystals (76%). ^{1}H NMR (C_6D_6, 25 °C): δ = 2.07 (s, 60H, C_5Me_5), 0.00 (s, 12H, ZnMe); ^{13}C NMR (C_6D_6, 25 °C): δ =110.91 (s, C_5Me_5), 13.21 (s, ZnMe), 10.96 (s, C_5Me_5). Elemental Anal. Calcd for $C_{44}H_{72}Zn_8Ni$: C, 44.68; H, 6.14; Zn, 44.23; found: C, 44.19; H, 6.19, Zn, 44.10; no gallium was detected.

[Pd(ZnCp*)$_4$(ZnMe)$_4$] (10). Compound **10** was prepared analogously to **9** as described above by using [Pd(GaCp*)$_4$] instead of [Ni(GaCp*)$_4$]. Yield: 75% white crystals. ^{1}H NMR (C_6D_6, 25 °C): δ = 2.08 (s, 60H, C_5Me_5), 0.04 (s, 12H,); ^{13}C NMR (C_6D_6, 25 °C): δ =110.23 (s, C_5Me_5), 15.66 (s, Zn*Me*), 10.82 (s, C_5Me_5). Elemental Anal. Calcd for $C_{44}H_{72}Zn_8Pd$: C, 42.94; H, 5.90; Zn, 42.51; found: C, 43.28; H, 5.81, Zn, 42.11; no gallium was detected.

[Pt(ZnCp*)$_4$(ZnMe)$_4$] (11). Compound **11** was prepared analogously to **9** as described above by using [Pt(GaCp*)$_4$] instead of [Ni(GaCp*)$_4$]. Yield: 81% white crystals. ^{1}H NMR (C_6D_6, 25 °C): δ = 2.06 (s, 60H, C_5Me_5), 0.18 (s, 12H, ZnMe); ^{13}C NMR (C_6D_6, 25 °C): δ =109.92 (s, C_5Me_5), 22.03 (tr, Zn*Me*, ^2J(Pt−C) = 74.06 Hz), 10.82 (s, C_5Me_5). Elemental Anal. Calcd for $C_{44}H_{72}Zn_8Pt$: C, 40.06; H, 5.50; Zn, 39.65; found: C, 40.09; H, 5.71, Zn, 39.80

[Pt(ZnCp*)$_4$(ZnEt)$_4$] (12). Compound **12** was prepared analogously to **11** as described above by using $ZnEt_2$ instead of $ZnMe_2$. Yield: 85% yellow crystals. ^{1}H NMR (C_6D_6, 25 °C): δ = 2.10 (s, 60H, C_5Me_5), 1.57 (m, 6H, Zn-CH_2CH_3), 1.46 (m, 6H, Zn-CH_2CH_3), 0.41 (m, 8H, Zn−CH_2CH_3); Interestingly, the ^{13}C NMR spectrum points to the presence of two isomers: ^{13}C NMR (C_6D_6, 25 °C): δ =110.34 (s, C_5Me_5), 33.95 (s), 32.83 (s), 11.12 (s), 10.78 (s), 10.24 (s), 9.33 (s), Elemental Anal. Calcd for $C_{48}H_{80}Zn_8Pt$: C, 41.92; H, 5.86; Zn, 38.04; found: C, 41.44; H, 5.39, Zn, 38.52; no gallium was detected.

Theoretical Methods. The geometries of the molecules were optimized at the gradient corrected DFT level of theory using Becke's exchange functional[46] in conjunction with Perdew's correlation functional[47] (BP86) with the TURBOMOLE 5.80 program package.[48] Ahlrich's def2-TZVPP basis set[49] was used. The RI approximation[50] was applied using auxiliary basis functions.[51] Stationary points were characterized by the analytical calculation of the Hessian using TURBOMOLE's aoforce module.[52] This level of theory is denoted as RI-BP86/def2-TZVPP.

Energy decomposition analyses (EDA) were carried out using the ADF(2007.1) program package.[53] Uncontracted Slater-type orbitals (STOs) were employed as basis functions in SCF calculations.[54] Triple-ζ-quality basis sets were used, which were augmented by two sets of polarization functions, that is, p and d functions for the hydrogen atom and d and f functions for the other atoms. This level of theory is denoted as BP86/TZ2P. An auxiliary set of s, p, d, f, and g STOs was used to fit the molecular densities and to represent the Coulomb and exchange potentials accurately in each SCF cycle.[55] Scalar relativistic effects were considered using the zero-order regular approximation (ZORA).[56]

In the EDA, bond formation between the interacting fragments is divided into three steps, which can be interpreted in a plausible way. In the first step the fragments, which are calculated with the frozen geometry of the entire molecule, are superimposed without electronic relaxation yielding the quasi classical electrostatic attraction ΔE_{elstat}. In the second step the product wave function becomes anti symmetrized and renormalized, which gives the repulsive term ΔE_{Pauli}, termed Pauli repulsion. In the third step the molecular orbitals relax to their final form to yield the stabilizing orbital interaction ΔE_{orb}. The latter term can be divided into contributions of orbitals having different symmetry. This latter step is crucial for the present study. The sum of the three terms $\Delta E_{\text{elstat}} + \Delta E_{\text{Pauli}} + \Delta E_{\text{orb}}$ gives the total interaction energy ΔE_{int}:

$$E_{\text{int}} = \Delta E_{\text{elstat}} + \Delta E_{\text{Pauli}} + \Delta E_{\text{orb}}$$

Note that the latter is not the same as the bond dissociation energy, because the relaxation of the fragments is not considered in ΔE_{int}. The interaction energy, ΔE_{int}, together with the term ΔE_{prep}, which is the energy necessary to promote the fragments from their

(46) Becke, A. D. *Phys. Rev. A* **1988**, *38*, 3098.
(47) Perdew, J. P. *Phys. Rev. B* **1986**, *33*, 8822.
(48) Ahlrichs, R.; Bär, M.; Häser, M.; Horn, H.; Kölmel, C. *Chem. Phys. Lett.* **1989**, *162*, 165.
(49) Weigend, F.; Ahlrichs, R. *Phys. Chem. Chem. Phys.* **2005**, *7*, 3297.
(50) Ahlrichs, R. *Phys. Chem. Chem. Phys.* **2004**, *6*, 5119.
(51) (a) Eichkorn, K.; Treutler, O.; Häser, M.; Ahlrichs, R. *Chem. Phys. Lett.* **1995**, *242*, 652. (b) Eichkorn, K.; Weigend, F.; Treutler, O.; Ahlrichs, R. *Theor. Chem. Acc.* **1997**, *97*, 119. (c) Weigend, F. *Phys. Chem. Chem. Phys.* **2006**, *8*, 1057.
(52) Deglmann, P.; May, K.; Furche, F.; Ahlrichs, R. *Chem. Phys. Lett.* **2004**, *384*, 103.
(53) ADF2007.01, SCM, Theoretical Chemistry; Vrije Universiteit: Amsterdam, The Netherlands, http://www.scm.com.
(54) Snijders, J. G.; Baerends, E. J.; Vernooijs, P. *At. Nucl. Data Tables* **1982**, *26*, 483.
(55) Krijn, J.; Baerends, E. J. *Fit Functions in the HFSMethod*, Internal Report (in Dutch); Vrije Universiteit: Amsterdam, The Netherlands, 1984.
(56) (a) Chang, C.; Pelissier, M.; Durand, P. *Phys. Scr.* **1986**, *34*, 394. (b) Heully, J.-L.; Lindgren, I; Lindroth, E.; Lundquist, S.; Martensson-Pendrill, A.-M. *J. Phys. Chem. B* **1986**, *19*, 2799. (c) van Lenthe, E.; Baerends, E. J.; Snijders, J. G. *J. Chem. Phys.* **1993**, *99*, 4597. (d) van Lenthe, E.; Baerends, E. J.; Snijders, J. G. *J. Chem. Phys.* **1996**, *105*, 6505. (e) van Lenthe, E.; van Leeuwen, R.; Baerends, E. J.; Snijders, J. G. *Int. J. Quantum Chem.* **1996**, *57*, 281.
(57) te Velde, G.; Bickelhaupt, F. M.; Baerends, E. J.; van Gisbergen, S. J. A.; Fonseca Guerra, C.; Snijders, J. G.; Ziegler, T. *J. Comput. Chem.* **2001**, *22*, 931.
(58) Recent reviews about the EDA method and its application have been published by: (a) Bickelhaupt, F. M.; Baerends, E. J *Rev. Comput. Chem* **2000**, *15*, 1. (b) Lein, M.; FrenkingG. *Theory and Applications of Computational Chemistry: The First 40 Years*; Dykstra, C. E, Frenking, G., Kim, K. S., Scuseria, G. E., Eds.; Elsevier: Amsterdam, 2005; p 291.

equilibrium geometry to the geometry in the compounds, can be used to calculate the bond dissociation energy as $-D_e = \Delta E_{prep} + \Delta E_{int}$. Because we are not concerned with the bond dissociation energies in this paper we give only the values for ΔE_{int} and its contributing terms. Further details about the EDA can be found in the literature.[57,58]

Acknowledgment. This work is dedicated to Prof. Herbert D. Kaesz, University of California, Los Angeles (UCLA). The German Chemical Industry Fund supported this work by granting Ph.D. stipends for T.C. and T.B. Further support by the Ruhr University Research School (www.research-school.rub.de/) and by the German Research Foundation (DFG, project Fi- 502/24-1) is gratefully acknowledged. M.T. has been funded by a DFG/TÜBITAK program (Fi 502/22-1).

Supporting Information Available: Energy level diagrams of 1H, 5H, 7H, 10H; description of the bonding situation of 7H; most important occupied MOs of 7H; calculated structure of $[Zr(ZnH)_{14}]$; crystallographic details for all crystal structures; comparison of calculated and experimental bond lengths; details of the EDA of 5H, 7H, 9H, 10H and 11H. This material is available free of charge via the Internet at http://pubs.acs.org.

JA904061W